Development 133, 2517-2525 (2006) doi:10.1242/dev.02422

Identification of Epha4 enhancer required for segmental expression and the regulation by Mesp2

Yoshiro Nakajima[1], Mitsuru Morimoto[1], Yuki Takahashi[1], Haruhiko Koseki[2] and Yumiko Saga[1,*]

Somites provide the basic body plan for metameric axial structures in vertebrates, and establish the segmental features through the sequential gene expression in the presomitic mesoderm (PSM). A crucial protein for segment border formation is the bHLH transcription factor Mesp2, the expression of which is restricted to the anterior PSM. A gene candidate that is activated by Mesp2 is *Epha4*, as its expression pattern resembles *Mesp2* and is absent in Mesp2-null embryos. We have analyzed the enhancer region of *Epha4*, which is responsible for its expression in the anterior PSM, and identified an E-box containing region. Subsequent transgenic and transient luciferase analyses successfully determined that the presence of repeated E-box sequences is a minimum essential requirement for the expression in the anterior PSM. We also show that Mesp2 directly binds to the enhancer sequence of *Epha4*. Furthermore, the forced expression of Mesp2 in somitic cells results in the activation of *Epha4* and repression of the caudal gene *Uncx4.1*, which may trigger the events leading to the formation of abnormal somites and rostralized vertebra. In addition, ectopic *Mesp2* expression induces abnormally epithelialized structures, which support to the idea that Mesp2 induces the formation of segmental borders by activating genes that play roles in cellular epithelialization.

KEY WORDS: Mesp2, Epha4, Somitogenesis, Segmental border, Mox1, mouse

INTRODUCTION

Somites are basic structures that underlie the segmental body architecture in vertebrates. The mechanisms involved in the generation of serially segmental units are a fascinating model system that has been used by many developmental biologists to further our understanding of the temporal and spatial control of gene expression. Somite precursors are derived as paraxial mesoderm from the primitive streak or tailbud region and these cells then come under the control of the segmentation clock, in which Notch signal oscillation generates the periodicity (for reviews, see Aulehla and Herrmann, 2004; Bessho and Kageyama, 2003; Maroto and Pourquié, 2001; Pourquié, 2003; Rida et al., 2004; Saga and Takeda, 2001). Notch signaling is suppressed in the anterior PSM by a bHLH protein, Mesp2, and the anterior limits of the Mesp2 expression domain demarcate the next segmental border (Morimoto et al., 2005). Mesp2 is a key transcription factor for both segment border formation and for the generation of rostrocaudal patterning within somites (Saga et al., 1997; Takahashi et al., 2000). The expression of many genes is affected in the Mesp2-null embryo, in which the genes required for rostral property are suppressed but those required for the development of caudal properties are enhanced. Among these genes, only lunatic fringe (*Lfng*) has so far been shown to be a direct target of Mesp2 (Morimoto et al., 2005).

Since the *Mesp2* expression domain is very similar to that of *Epha4*, and this gene is also suppressed in the Mesp2-null embryo (Nomura-Kitabayashi et al., 2002), it was probable that Mesp2 directly activated *Epha4* in the rostral compartment of the somites. Furthermore, Epha4 is implicated in segmental border formation in zebrafish (Cooke et al., 2005; Barrios et al., 2003; Durbin et al., 1998), although gene knockout studies indicate that Epha4 is not the sole protein required for segmental border formation in the mouse, as no somitic phenotype has been reported (Dottori et al., 1998; Kullander et al., 2001) (M. Asano, personal communication). The identification of target genes for a transcription factor is necessary to understand fully the genetic networks involved in a particular biological system. However, it is very difficult to achieve these using straightforward methods such as SELEX or immunoprecipitation, particularly in embryonic tissues. As an alternative method, we attempted to first identify the *Epha4* enhancer and then test whether Mesp2 directly binds to this region; if it does not bind, we can search the binding protein that might be a direct target of Mesp2. Fortunately, the *Epha4* enhancer elements identified showed direct binding to Mesp2, together with E47 (Tcfe2a – Mouse Genome Informatics) in vitro. Moreover, the forced expression of Mesp2 resulted in the reverse phenotype of the Mesp2-null embryo, whereby *Epha4* is activated, *Uncx4.1* is suppressed and ectopic epithelialization could be observed in the transgenic embryos.

MATERIALS AND METHODS

Construction of lacZ reporter constructs

An 8.8 kb fragment (*Nhe*I-*Xba*I) was isolated from an *Epha4*-containing bacterial artificial chromosome clone (415B3) and subcloned into the pBluescript vector (Stratagene). A series of deletion constructs were then generated using the appropriate restriction enzymes (Fig. 1A). These genomic fragments were inserted into a *lacZ* reporter vector, upstream of the hsp promoter (Kothary et al., 1989). E-box deletion and mutant constructs were subsequently generated via PCR using the 630 bp enhancer region (*Hin*dIII cut) as a template (Imai et al., 1991).

Formation of E-box multimer constructs

Synthetic oligonucleotides were designed to generate two repeats of 20 bp containing an E-box when annealed (Fig. 2C). These E-box-containing sequences were flanked by *Bgl*II and *Bam*HI sites. The complementary oligonucleotides were annealed and phosphorylated with T4 polynucleotide kinase prior to ligation. Ligated DNA were digested with *Bam*HI and *Bgl*II, and separated on 2% agarose gels. Multimerized bands were excised and subcloned into the pBluescript vector.

[1]Division of Mammalian Development, National Institute of Genetics, Yata 1111, Mishima 411-8540, Japan. [2]Division of Developmental Genetics, RIKEN Research Center for Allergy and Immunology (RCAI) RIKEN Yokohama Institute, 1-7-22 Suehiro, Tsurumi-ku, Yokohama 230-0045, Japan.

*Author for correspondence (e-mail: ysaga@lab.nig.ac.jp)

Accepted 2 May 2006

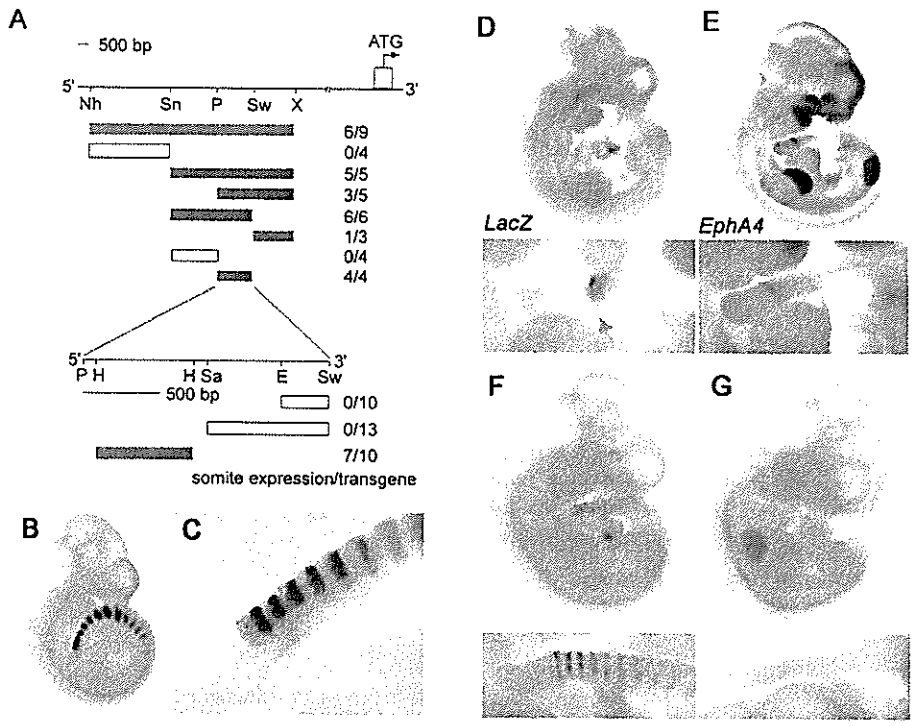

Fig. 1. Identification of a somite-specific *Epha4* enhancer. (**A**) The *lacZ* transgene constructs used to identify the cis-acting somite enhancer within the *Epha4* genomic region. The numbers of transgenic mouse embryos that expressed β-gal in the somites, among the transgene-positive embryos, are indicated on the right. E, *Eco*RI; H, *Hin*dIII; N, *Nhe*I; Sa, *Sac*I; Sw, *Swa*I; P, *Pma*CI; X, *Xba*I. (**B,C**) Lateral view of β-gal activity driven by the 630 bp (*Hin*dIII) *Epha4* enhancer fragment in a 10.5 dpc embryo. A magnified image in the somitic region of B is shown in C. (**D,E**) Comparison by in situ hybridization at 10.5 dpc of the transgene expression (*lacZ*) in a transgenic embryo (D) with endogenous *Epha4* expression in the wild-type embryo (E). In situ signals in the anterior PSM are indicated by arrows in the lower panels showing magnified images. (**F,G**) β-Gal activity driven by the 630 bp enhancer in 10.5 dpc wild-type (F) and $Mesp2^{t/t}$ embryos (G).

Generation of transgenic mice

All constructs were digested with restriction enzymes to remove vector sequences and then gel purified. Transgenic mice were generated by microinjection of fertilized eggs. Microinjected eggs were transferred into the oviducts of pseudopregnant foster females. The genotypes of the embryos were identified by PCR using DNA prepared from the yolk sac.

Luciferase assay

An *Epha4* somite enhancer insert (630 bp *Hin*dIII-*Hin*dIII fragment) and E-box multimers were cloned into the pGL3-Promoter vector (Promega). NIH3T3 cells were grown at 80% confluency in 24-multiwell plates and transfected with luciferase gene constructs using Lipofectamine Plus (Invitrogen). Cells were harvested 36 hours after transfection and luciferase activities were measured using a Dual Luciferase Assay Kit (Promega). The transfection efficiency was normalized by co-transfection of the Renilla luciferase expression vector pRL-TK (Promega), and the relative luciferase activity was determined as recommended by the manufacturer.

Electrophoretic mobility shift assay (EMSA)

For protein preparation, NIH3T3 cells were grown at 80% confluency in 10 cm dishes and transfected with expression vectors containing either 3×FLAG-tagged Mesp2 or Myc-tagged E47. Nuclear extracts were prepared using Nuclear Extract Kit (Active Motif). The protein concentrations were measured by the Bradford assay (Pierce). EMSA was performed using a DIG gelshift and detection kit (Roche). Binding reactions were carried out by mixing DIG-labeled and unlabeled (for competition experiments) probes with nuclear extracts from NIH3T3 cells. In experiments using antibodies, the nuclear extracts were preincubated with the antibody for 1 hour on ice.

Generation of *CAG-CAT-Mesp2* transgenic and *Mox1-cre* knock-in mice

A targeting vector was designed to introduce the *Cre* gene near to the translational initiation site of the *Mox1* gene (see Fig. S1 in the supplementary material) and used to establish the *Mox1-cre* mouse line, in which Cre recombinase is expressed instead of Mox1 and the gene activity is examined by crossing with a reporter line, R26R (Zambrowicz et al., 1997). To achieve the ectopic expression of Mesp2, a *CAG-floxed-CAT-Mesp2* transgene was constructed (Yamauchi et al., 1999), in which *CAT* gene can be excised by Cre recombinase and thus the *Mesp2* gene comes under the control of the *CAG* promoter (see Fig. S1 in the supplementary material). Transgenic mouse lines were established by microinjection of *CAG-floxed CAT-Mesp2* DNA as described above.

Analyses of embryos by LacZ staining, in situ hybridization, skeletal and the histological methods

Embryos were fixed and stained in X-gal solution for the detection of β-gal activity, as described previously (Saga et al., 1999). For histology analyses, samples stained by X-gal were postfixed with 4% paraformaldehyde, dehydrated in an ethanol series, embedded in paraffin and sectioned at 6 μm. Whole-mount in situ hybridization was performed using InsituPro robot (Intavis). The transcripts were visualized using anti-digoxigenin (DIG) antibodies conjugated to alkaline phosphatase. Color reactions were performed using BM Purple (Roche). Methods employed for section in situ hybridization and for the immunohistological detection of Mesp2 have been previously described (Morimoto et al., 2005). Skeletal preparations by Alcian Blue/Alizarin Red staining have also been described previously (Saga et al., 1997; Takahashi et al., 2000). Probes used for the in situ hybridization detection of *Uncx4.1* and *Sox9* were kindly provided by Dr Peter Gruss and Dr Veronique Lefebvre, respectively. For the detection of actin filaments, frozen sections were stained with AlexaFluor 488-conjugated phalloidin (Molecular Probes) according to the manufacturer's protocol.

RESULTS

Enhancer analysis of *Epha4*

Previous enhancer studies have indicated that a somite specific enhancer is not contained within the 7.5 kb region upstream of the *Epha4* transcriptional start site, in which only rhombomere-specific enhancer activity has been identified (Theil et al., 1998). To identify the somite specific enhancer region of the *Epha4* gene, we focused on the more upstream region of the gene. We subsequently found the enhancer within an 8.8 kb fragment, beginning 8 kb upstream of the *Epha4* transcriptional start site (Fig. 1A). β-Gal activity was observed in the rostral compartment of the segmented somites (Fig.

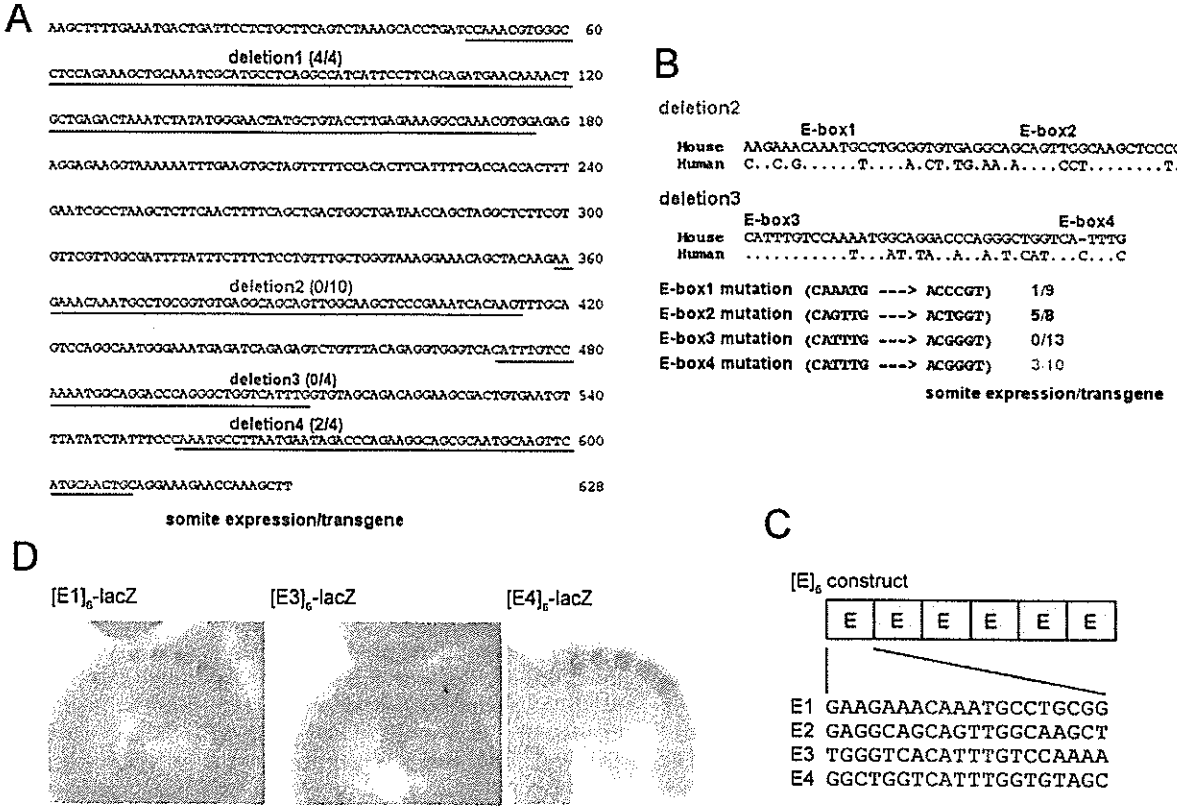

Fig. 2. Identification of the functional E-box motifs responsible for the somite-specific activation of *Epha4*. (**A**) Sequence of the 630 bp *Epha4* somite enhancer (core enhancer) region. The four indicated fragments (fragment 1-4) represent deleted sequences from the core enhancer region. The results of transgenic analyses using these deleted constructs are shown in parentheses. (**B**) Sequence alignment of somite enhancer regions (fragment 2 and fragment 3) of mouse *Epha4* with the corresponding regions of human *Epha4*. The mutations introduced in each E-box and the results of the subsequent transgenic analyses are shown. (**C**) Schematic representation of artificially constructed enhancers, containing six E-box motif repeats. (**D**) The artificial enhancers were cloned upstream of a *lacZ* reporter vector and the results of the subsequent transgenic analyses (representative images are shown) are indicated in parentheses. For the $[E2]_6$-lacZ artificial enhancer, no somite expression was observed among the 11 transgene-positive embryos. Blue letters indicate putative E-box motifs.

1B,C), and to confirm that this reflects endogenous *Epha4* expression, we compared the expression of *lacZ* RNA with the endogenous *Epha4* transcripts. Among several expression domains of endogenous *Epha4*, such as limb buds, branchial arches and rhombomeres, an identical expression pattern was revealed in both the anterior PSM and the rostral compartment of the S1 somites (Fig. 1D,E). Further transgenic analyses were conducted using DNA fragments that had been generated by several restriction enzymes. Although we detected one embryo which showed somite-specific expression using Sw-X region, we concentrated our analyses on the P-Sw region, which showed most consistent results. Further deletion identified a *Hin*dIII fragment of 630 bp that could sustain endogenous pattern of somite-specific *Epha4* expression (Fig. 1A). We established a permanent transgenic line using a *lacZ* reporter with the 630 bp enhancer. The somite-specific expression was observed during somitogenesis from 8.5 to 11.5 days post-coitum (dpc) as similar to the endogenous one (see Fig. S2 in the supplementary material). However, the transgene expression became weaker in the later stage embryo at 11.5 dpc and the somite-specific expression was not observed with both probes for endogenous *Epha4* and *lacZ* transgene after 13.5 dpc (data not shown). When the expression was examined in the *Mesp2*-null genetic background ($Mesp2^{LL}$) (Takahashi et al., 2000), no β-gal activity was detected in the $Mesp2^{LL}$ embryos (Fig. 1F,G), which confirms that the enhancer contains cis elements required for the *Epha4* activation downstream of the Mesp2.

Subsequent sequence analysis revealed that this 630 bp region contained eight E-boxes. As Mesp2 belongs to the bHLH family of transcription factors, which are known to bind E-box or N-box motifs, we initially performed deletions of some of the *Epha4* E-boxes. We generated four deletion constructs that lack a region (fragments 1-4) of the E-boxes (Fig. 2A) and examined the enhancer activities. Our results clearly showed that the enhancer activity was completely lost when using both fragment 2- and 3-deletion constructs, indicating that both regions are necessary for its expression (Fig. 2A). Both fragments 2 and 3 contain two E-boxes, designated E1- E4 (Fig. 2B). The core sequences of E1, E3 and E4 are identical (CAAATG or CATTTG) but only E1 and E3 are conserved in the human *EPHA4* gene. To determine whether these E-boxes are crucial, we next introduced mutations into their consensus sequences and transgenic analysis was conducted using the full 630 bp enhancer as a wild-type activity control. The E2 mutation did not affect enhancer activity but a considerable reduction in the activity was observed for the E1 and E3 mutations. In addition, mutation of E4 substantially disrupted enhancer activity, indicating that a mutation in a single E-box abrogates the enhancer

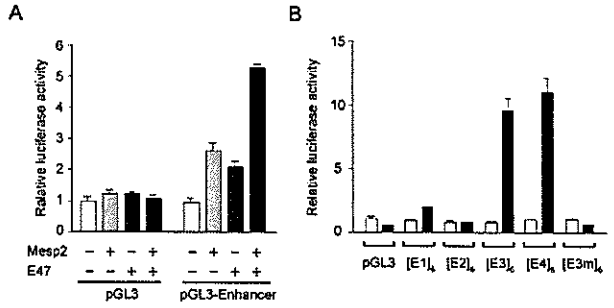

Fig. 3. Transactivation of the *Epha4* enhancer by the Mesp2/E47 heterodimer. *Epha4* somite enhancers (A, 630 bp core sequence; B, six tandem repeats of E-box sequences) were ligated to the pGL3 luciferase vector. Luciferase activity was measured at 36 hours after transfection into NIH3T3 cells. (**A**) The presence (+) or absence (–) of either Mesp2 or E47 are indicated in each column. (**B**) Luciferase activity was compared with (black bars) and without (white bars) Mesp2/E47. Mutations in E3 (5′-CATTTG-3′), that give rise to E3m (5′-ACGGGT-3′), results in the loss of reporter activity. The results shown are the mean values from three independent experiments. Standard deviations are indicated by error bars.

activity and that the presence of tandem repeats of the E-box consensus sites is important for the activity. To confirm this, we generated reporter constructs with artificial enhancers, composed of six tandem repeats of the E1, E2, E3 or E4 boxes and flanking sequences (Fig. 2C). Transient transgenic analysis revealed that each of these regions, with the exception of E2, showed weak but specific expression in the somitic region (Fig. 2D). This confirmed that these E-boxes are a minimum requirement for the specificity of *Epha4* expression in the somitic region and that the consensus sequence is CAAATG.

The *Epha4* enhancer is activated by Mesp2 in cultured cells

The identification of E-boxes as a vital component of the *Epha4* enhancer strongly indicates that this gene is directly regulated by Mesp2, as the bHLH-type transcription factor is known to bind E-boxes. In order to further elucidate whether Mesp2 can activate the *Epha4* enhancer, we established a luciferase assay system using NIH3T3 cultured cells. The reporter gene was constructed by ligating the 630 bp *Epha4* enhancer region to a luciferase gene. As B-type bHLH transcription factors are known to function as heterodimers with the so called A-type bHLH factors (Ledent and Vervoort, 2001), we analyzed reporter activity with or without E47, which is a typical A-type bHLH factor. As shown in Fig. 3A, Mesp2 and E47 alone exhibited weak transactivating activities when these expression vectors were separately transfected with the reporter construct, whereas strong activity was observed when Mesp2 and E47 were co-transfected. The transactivating activity of Mesp2 alone can be ascribed to its association with endogenous E47. Next, we constructed reporters with six repeats of each of the *Epha4* enhancer E-boxes (E1 to E4) used in our transgenic analyses (Fig. 2C). Interestingly, very strong activity was observed when the E3 and E4 constructs were used, and this was only observed upon co-transfection with E47 (Fig. 3B). This specificity was confirmed by the lack of activity resulting from a construct with a mutant-type E3 enhancer element. E2 showed no activity, which is consistent with the findings of our transgenic analysis. E1 did not have strong activity, although we obtained positive activity for this E-box via transgenic analysis.

The binding abilities of Mesp2 and E47 to the *Epha4* E-boxes were then analyzed using electrophoresis mobility shift assays (EMSA). Nuclear extracts were prepared from NIH3T3 cells, transfected with either FLAG-tagged Mesp2 or Myc-tagged E47, and these were used in the experiments either separately or in combination. The E3 motif was used in the EMSA experiments as it gave the most consistent results in both the transgenic and luciferase assays. As expected, a strong bandshift was observed when both Mesp2 and E47 were combined, although a faint band was detectable when E47 was incubated alone, indicating that it may form a homodimer that can bind the E3 E-box (Fig. 4A). The sequence specificity of the protein-DNA interactions was confirmed by competition assay using both intact and mutated sequences (Fig. 4B). The specificity of the heteroduplex complex was also confirmed by supershift experiments with anti-FLAG and anti-Myc antibodies (Fig. 4C). We also examined the binding specificity by applying other bHLH proteins. A family protein, Mesp1 also showed strong

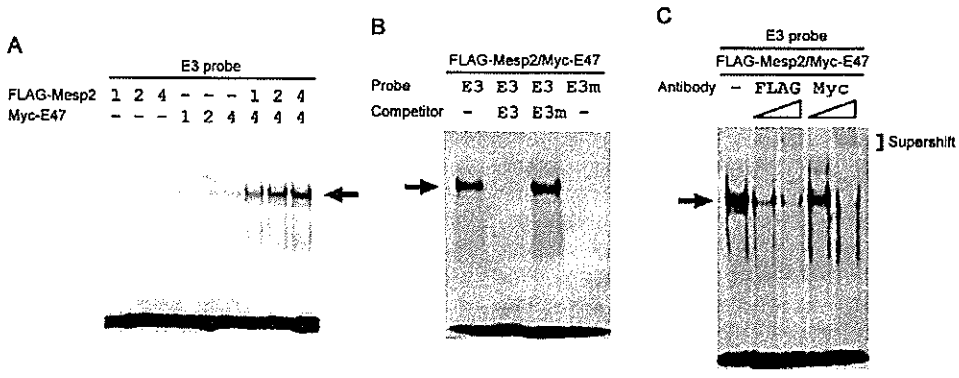

Fig. 4. The Mesp2/E47 heterodimer binds to the E3 site of the *Epha4* enhancer. (**A**) The results of EMSA using nuclear extracts from NIH3T3 cells transfected with FLAG-Mesp2 and/or Myc-E47 and incubated with E3 probe. The quantities of nuclear extracts used (μg) are indicated. (**B**) A competition assay indicating the specificity of the binding of the Mesp2/E47 (2 μg each) complex to the E3 probe. The addition of 100-fold excess of unlabeled E3 probe, but not the E3m mutant probe, abolished the binding. (**C**) Evidence for the heterodimer formation of FLAG-Mesp2/Myc-E47. The band containing E3 (arrow) was supershifted by the addition of either anti-FLAG or anti-Myc antibodies. The oligonucleotides used were as follows: E3, 5′-TGGGTCA**CATTTG**TCCAAAA-3′; E3m, 5′-TGGGTCAACGGGTTCCAAAA-3′ (E-box is shown in the bold; altered nucleotides in the mutant probe are underlined).

binding, but other bHLH proteins such as paraxis (Tcf15 – Mouse Genome Informatics), Myod1 and Twist (Twist1 – Mouse Genome Informatics) did not show significant binding to the E3 probe (see Fig. S3 in the supplementary material). These data strongly suggest that Mesp2 forms a heterodimer with E47, binds to the E-boxes within the *Epha4* enhancer and then activates *Epha4* transcription in the rostral region of somites.

The overexpression of *Mesp2* leads to the activation of *Epha4*

Epha4 has been implicated in border formation via the repulsive interaction with ephrin molecules, and this occurs during the formation of segmental boundaries in the hindbrain and in the somites (Barrios et al., 2003; Cooke et al., 2005; Durbin et al., 1998). However, loss-of-function experiments have failed to show any functional relevance for Epha4 in the mouse. In order to investigate whether Mesp2 functions as an activator of *Epha4*, and possibly to reveal the role of Epha4 during somitogenesis, we established a system that achieves the conditional expression of Mesp2 using Cre-loxP. A transgenic mouse line *CAG-floxed-CAT-Mesp2* was established in our laboratory, in which the *CAT* gene is inserted between two *loxP* sites and can therefore be excised by Cre recombinase. Hence, the *Mesp2* gene in this system will come under the control of the *CAG* promoter after this excision. To activate *Mesp2*, we generated and then used a *Mox1-Cre* mouse (see Fig. S1 in the supplementary material). *Mox1* expression initiates just prior to segment border formation, in a similar manner to endogenous *Mesp2*, but its expression persists after segmentation and is relatively higher in the caudal half of the somites (Mankoo et al., 2003; Saga et al., 1997) (Fig. 5A,B). The *Cre* expression was detected as early as 8.5 dpc and showed the similar pattern to the *Mox1* (Fig. 5C-E).

To confirm the presence of Cre recombinase activity, we crossed the *Mox1-Cre* mouse with the R26R reporter line and examined β-gal activity during the period 8.5-11.5 dpc (Fig. 5F-I; data not shown). The expression of the reporter was found to begin in the paraxial mesoderm and the most prominent levels were restricted to the somitic derivatives, at least up to 11.5 dpc. Some reporter expression in the rostral neural tube and in the intermediate mesoderm was also observed. We detected differences in the initial expression domain between the *Mox1* (Fig. 5B) or *Cre* transcripts (Fig. 5E), and β-gal reporter activity (Fig. 5G), which most likely reflects a time-lag for the activation of the reporter gene following the excision of the *CAT* gene by Cre recombinase. Histological sections revealed that the reporter activation was initiated in only a few somitic cells just after segmentation, but that the β-gal expression gradually expanded throughout the entire components of somite derivatives. Hence, this Cre line is a useful system to drive genes in the somitic cell lineage.

Mesp2 activation induces abnormal epithelialization

To activate *Mesp2* expression in the somitic lineage, we crossed the *CAG-CAT-Mesp2* and *Mox1-cre* lines. The double heterozygous mice died shortly after birth and their skeletal specimens revealed strong malformations (see below), indicating abnormal somitogenesis. Under a dissection microscope, the morphology of the somites was not found to have been disrupted, which was unexpected from the observations of the skeletal phenotype. Segmental boundaries were observed, although their width was not perfectly equal to the wild type and the surface appeared to be rough. At first, we analyzed *Mesp2* expression at 10.5 dpc (Fig. 6A,B). In

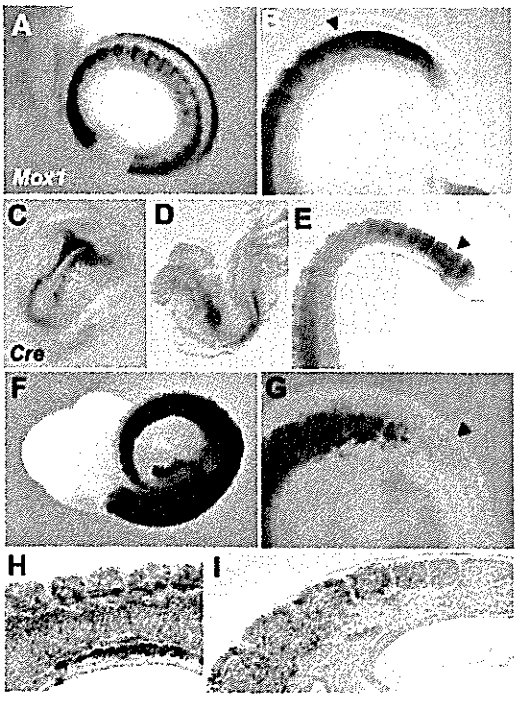

Fig. 5. *Mox1* and *Mox1-cre* expression and the lineage analysis. Whole-mount in situ hybridization analysis of *Mox1* expression in 9.5 dpc embryos (**A**,**B**) and *Mox1-cre* in 8.25 (**C**), 8.5 (**D**) and 11.5 (**E**) dpc embryos. (**F-I**) Whole-mount expression patterns and sagittal sections of β-gal-stained *R26R/Mox1-cre* double heterozygous embryos at 10.5 dpc. (H,I) The sections were counterstained with Eosin. Arrowheads indicate somite borders forming between S0 and S-1.

the wild-type and single heterozygous embryos, *Mesp2* is expressed in the anterior PSM as a single band, although the width and the strength of this expression differs from embryo to embryo as shown previously (Fig. 6A) (Takahashi et al., 2000). In double heterozygotes, however, the ectopic expression of *Mesp2* could be observed throughout the entire somitic region, in addition to its normal expression pattern in the anterior PSM (Fig. 6B). Moreover, the *Mesp2*-positive cells often formed clusters and were not localized in specific regions of somites (Fig. 6C,D).

A similar ectopic expression pattern was observed for *Epha4*, although the levels of ectopic expression were much lower than the endogenous gene expression (Fig. 6E-H). The spotty expression pattern in both *Mesp2* and *Epha4* indicates that the expression is suppressed or the transcripts are destabilized in many cells and only parts of cells maintain the expression. To further investigate the characteristics of the gene expression profiles and morphologies, serial sections were prepared and subjected to staining for Mesp2 protein, *Epha4* transcripts and actin filaments (Fig. 6I-N). The segmental borders were found to have generated but fluorescent phalloidin staining revealed cells showing abnormal epithelialized features and broken epithelial sheaths were also evident (Fig. 6N). In the cells nearby, both ectopic Mesp2 (Fig. 6K) and *Epha4* expression (Fig. 6L) could be observed. Although we could not conclude that Mesp2 directly induced *Epha4* using the serial sections, these observations indicate that the cells may have acquired repulsive properties that enable them to form abnormal cell borders within somites (Fig. 6O).

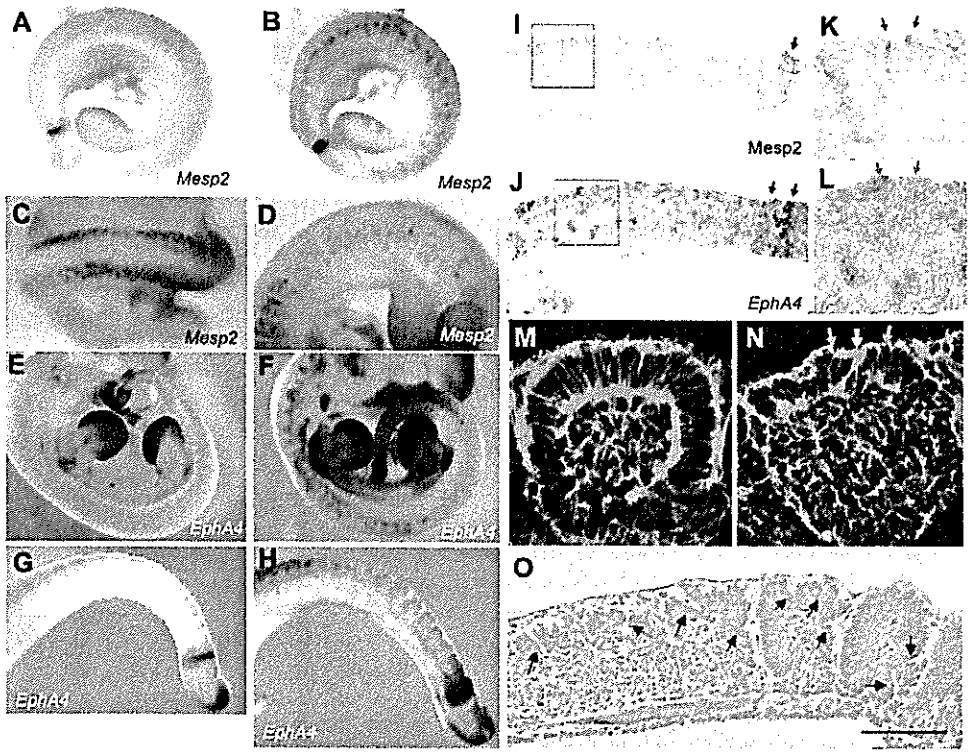

Fig. 6. Ectopic Mesp2 expression in somites leads to the activation of *Epha4*. Expression of *Mesp2* in 10.5 dpc wild-type (**A**) and *CAG-CAT-Mesp2; Mox1-Cre* double heterozygous embryos (**B-D**). In addition to the normal *Mesp2* expression in the anterior PSM, ectopic expression of *Mesp2* was observed throughout the entire somitic region (B-D). The expression pattern of *Epha4* at 11.5 dpc in wild-type (**E,G**) and double heterozygous embryos (**F,H**) is also shown. An expression pattern for *Epha4* that was similar to *Mesp2* was observed in the double heterozygote (F,H). Histological analyses of 10.5 dpc wild-type (**M**) and double heterozygous (**I-L,N**) embryos. Ectopic Mesp2 protein (I,K) and *Epha4* expression (J,L) were evident in serial sections of double heterozygotes. Magnified images of square parts of I and J are shown in K and L, respectively. Another consecutive section was stained with phalloidin (N) and a similar region of the wild-type embryo is shown in M. In double heterozygotes, abnormal epithelial cells were observed within the somite (N). A paraffin section stained with nuclear Fast Red revealed gaps in epithelialized somites in the double heterozygote at 10.5 dpc (**O**). Black arrows in I and J indicate the endogenous expression of Mesp2 (I) or *Epha4* (J). Red arrows in K,L,N indicate separated cell clusters. White arrow in N indicates an abnormal epithelialized feature. Black arrows in O indicate local gaps. Scale bar: 100 μm.

Mesp2 activation induces skeletal malformation

The *CAG-CAT-Mesp2/Mox1-Cre* double heterozygous fetus showed strong skeletal defects, which are restricted in the ribs and vertebra as expected from the somite-specific *Mox1* expression (Fig. 7A-H) (Mankoo et al., 2003). The vertebral bodies and the lamina of neural arches were present in these fetuses, although they displayed severe defects in both their morphology and patterning. By contrast, the pedicles of the neural arches were largely lost (Fig. 7C,G). In addition, the proximal region of the ribs did not form properly (Fig. 7D,H). This phenotype contrasts with Mesp2-null embryos and is somewhat similar to Psen1-null mutants (Takahashi et al., 2000), indicating that it is a rostralized phenotype. To gain insight into the morphogenetic failure underlying the skeletal defects observed in the double transgenic mice, cartilage formation was examined by whole-mount staining with Alcian Blue. Strikingly, rib as well as pedicle cartilages were severely affected even in the 13.5 dpc embryo (Fig. 8A,B).

Mesp2 is required for the establishment of the rostral properties within somites via the suppression of caudal genes. Therefore, we anticipated that the forced expression of Mesp2 may lead to the suppression of caudal properties, which would be the cause of the skeletal malformation. *Uncx4.1* is a molecular marker for caudal somites (Fig. 8C,E,G) and this gene is also known to be required for the pedicle formation of the neural arch (Leitges et al., 2000; Mansouri et al., 2000). In the *CAG-CAT-Mesp2/Mox1-Cre* double heterozygotes, the caudally restricted expression pattern was not disrupted but the levels of expression were much lower and the stripes were often interrupted (Fig. 8D,F). The histological section revealed the presence of signal-negative regions in the caudal compartments, which was often accompanied by the morphological abnormalities. We noticed local fusion between cells in the caudal compartment and the rostral ones in the posterior somite (Fig. 8H). Such a fusion was never observed in wild-type or single heterozygous embryos (Fig. 8G).

To explore more genes affected in Mesp2-activated embryos and to understand the cause of abnormalities, we examined expressions of several somitic markers at 11.5 dpc. The segmental expression of *Pax3* that is the marker of dermomyotome (Fig. 8I) (Denetclaw and Ordahl, 2000) was expanded in the double transgenic embryo (Fig. 8J), which may indicate expansion of the dermomyotomal progenitor. By contrast, *Sox9*-positive cell lineage appeared to be

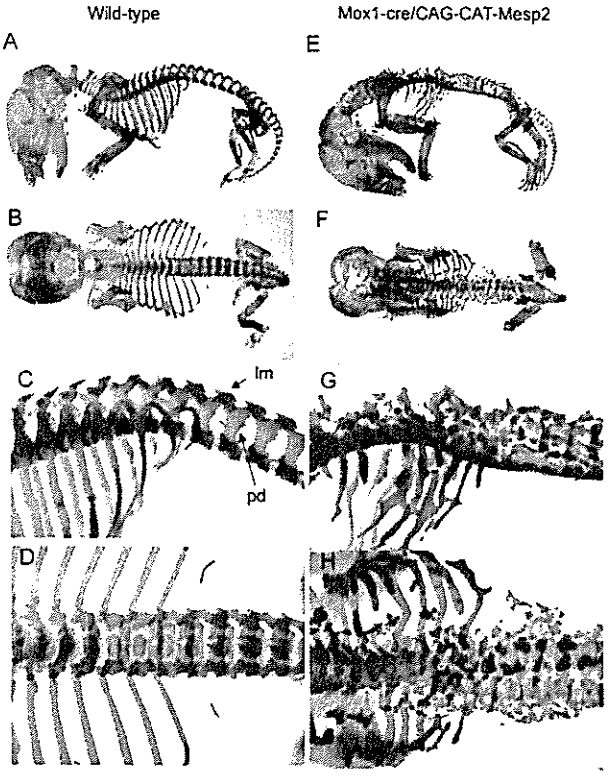

Fig. 7. Ectopic expression of Mesp2 leads to skeletal malformations. Skeletal preparations of 18.5 dpc wild-type (**A-D**) and *CAG-CAT-Mesp2; Mox1-Cre* fetuses (**E-H**) stained with Alcian Blue and Alizarin Red. Lateral (A,E) and dorsal (B,F) views of whole skeletons are shown. Higher magnifications of the lumber region from wild-type (C,D) and double heterozygous fetuses (G,H) are also shown. The lack of pedicles of the neural arches could be observed in the double heterozygotes (G,H). The rib structure was also severely affected in the double heterozygotes (G,H). pd, pedicle; lm, lamina.

relatively reduced in the transgenic embryo especially in the thoracic region (Fig. 8K,L), which may account for the underdevelopment of the rib cartilage. The expansion of the rostral compartment of somites was indicated by the expression of *Tbx18* (Fig. 8M-P), which is another target candidate of Mesp2 as its expression is lost in the *Mesp2*-null embryo (Bussen et al., 2004) (Y.T., unpublished).

These observations are consistent with the idea that ectopic Mesp2 expression is of sufficient strength to activate rostral genes such as *Epha4* and *Tbx18*, and to suppress expression of the caudal gene *Uncx4.1*.

DISCUSSION

In our current study, we have identified a cluster of E-boxes in the enhancer region of *Epha4*, incorporating the Mesp2 binding site, in which at least three crucial E-boxes (E1, E3 and E4 in Fig. 2C) are present. The loss of these motifs results in a substantial reduction in gene reporter activity, in both luciferase and transgenic reporter assays, indicating that there is an essential requirement of multiple E-boxes for *Epha4* activation by Mesp2. Interestingly, the co-expression of Mesp2 and E47 resulted in higher luciferase activity (tenfold) (Fig. 3B), whereas only weak activity (twofold) was obtained with Mesp2 alone (data not shown). Mesp2 alone could also not bind to E-box containing DNA sequences (Fig. 4A). Therefore, Mesp2 alone or Mesp2 homodimers appear to be inactive on *Epha4* somite enhancer.

The core E-box sequence appears to be CAAATG/CATTTG and synthetic enhancers generated by six repeats of the *Epha4* enhancer E1, E3 and E4 motifs, and flanking sequences, can recapitulate the segmental expression pattern of this gene in vivo. The differences that we observed in the measured luciferase activities for the multiple E-boxes may reflect the involvement of the sequences flanking the core enhancer region in promoting the binding of bHLH-type transcription factors, which has been observed in other cases (Powell et al., 2004). In addition, other factors may modulate the interactions between Mesp2/E47 and its target sequences. It has been reported that the phosphorylation of E47 is required for the formation of heterodimers with Myod1 and for the subsequent binding to the target sequence (Lluis et al., 2005). The methylation state of target sequences has also been implicated in the binding by another bHLH heterodimer, Max/Myc, in which methylation of the CpG dinucleotide within the E-box has been shown to prevent the access of the bHLH proteins (Perini et al., 2005). Further studies will be required to determine whether such modulations are involved in the binding of the Mesp2/E47 heterodimer to its target sites.

Epha4 is implicated in segmental border formation via its interaction with the Eph ligand ephrin, which is expressed in apposed cells in zebrafish (Barrios et al., 2003; Durbin et al., 1998). However, there is no direct evidence for this in the mouse, as the loss of Epha4 failed to reveal any role for this protein during somitogenesis, which may be due to functional redundancy among the several Eph and ephrin family proteins. In such a situation, a transgenic strategy of forced gene expression is an alternative and effective method. In the current study, we have tried the forced expression of *Mesp2* with expectation that *Epha4* should be induced under the control of Mesp2. The forced expression of Mesp2 not only activates *Epha4* expression but also induces the local segregation of somitic cells. Recently, we showed that Mesp2 establishes the segmental boundary by suppressing Notch signaling, which then generates a boundary between the Notch-active and Notch-negative domains (Morimoto et al., 2005). We have also shown that this boundary forms the next somite border. However, the precise molecular mechanisms involved in the generation of these morphological boundaries are not yet fully understood, although Cdc42 and Rac1 are known to play important roles in subsequent epithelial somite formation (Nakaya et al., 2004). Although the direct evidence was not presented, our current data indicate that Mesp2 activates *Epha4* in the anteriormost cells in the PSM and that this may activate reverse signaling though ephrin expression in opposing cells and generate a gap during normal somitogenesis. A similar mechanism has previously been proposed for the epithelialization of boundary cells in zebrafish (Barrios et al., 2003; Cooke et al., 2005). Nevertheless, we can not exclude the possibility that pathways other than Epha4 activation by Mesp2 are required for the induction of epithelialization.

Mesp2 is also known as a strong suppressor of the establishment of caudal properties, which is mediated by the suppression of both Notch signaling and *Dll1* and *Uncx4.1* expression (Nomura-Kitabayashi et al., 2002; Takahashi et al., 2000). We actually did observe suppression of *Uncx4.1* in our double heterozygotes, but the segmental pattern of *Uncx4.1* expression at 10.5 dpc was not found to be severely disrupted. Therefore, our finding of an extremely defective skeletal phenotype in the *CAG-CAT-Mesp2/Mox1-Cre*

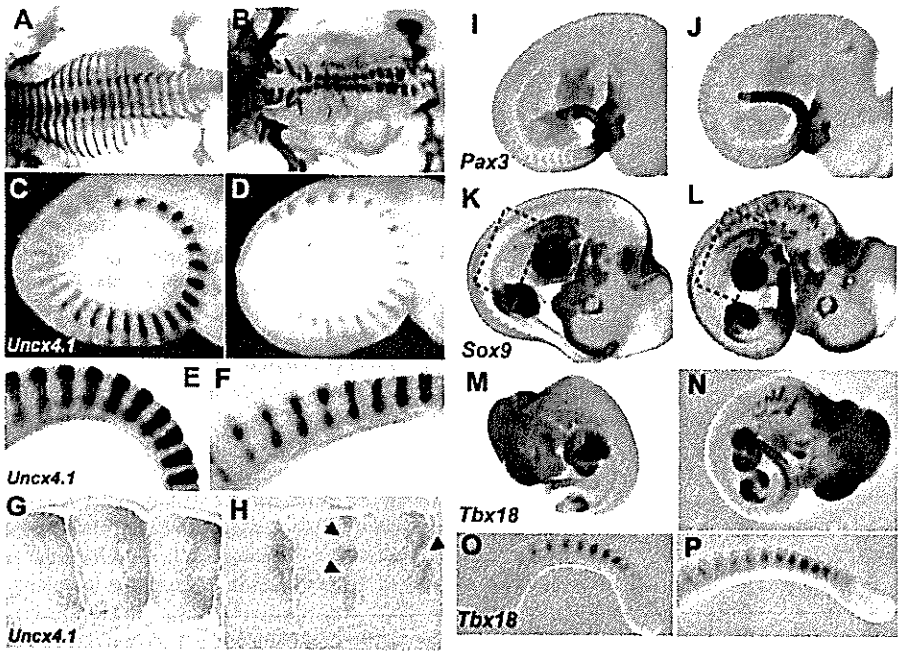

Fig. 8. Early defects in chondrogenesis and gene expressions affected in the *CAG-CAT-Mesp2;Mox1-Cre* double heterozygotes. Skeletal morphology was revealed by Alcian Blue staining in the wild-type (**A**) and double heterozygous (**B**) embryos at 13.5 dpc. (**C-H**) *Uncx4.1*. expression was reduced in double heterozygotes (D,F) at both 10.5 (C,D) and 11.5 dpc (E,F) compared with wild-type embryos (C,E). The section of 11.5 dpc embryonic tail revealed *Uncx4.1*-negative cells (arrowheads) in the caudal compartment of somites in the double heterozygote (H). Comparison of expression patterns of *Pax3* (**I,J**), *Sox9* (**K,L**) and *Tbx18* (**M-P**) between wild-type (I,K,M,O) and double heterozygous (J,L,N,P) embryos. Outlines in K and L show *Sox9* expression in the rib primordia.

mice was somewhat surprising. We postulate that prolonged Mesp2 expression, driven by the CAG promoter, must continuously attenuate *Uncx4.1* and the corresponding downstream gene expression in the later stages of development, which would lead to the almost complete suppression of chondrogenesis, as observed in the case of loss of Uncx4.1 (Leitges et al., 2000; Mansouri et al., 2000). One of target genes activated by Uncx4.1 and responsible for the phenotype would be *Sox9*, the product of which is known to be a key regulator of chondrogenesis (Akiyama et al., 2005). However, it remains to be investigated whether this suppression is directly mediated by Mesp2 or by other transcriptional suppressors that are activated by Mesp2.

We also show in our present study that the *Mox1-Cre* mouse is a useful tool for inducing either the disruption or activation of genes that are components of the somitic cell lineage. However, there is a delay in gene activation and the activation of *Mesp2* was 'spotty' and these may be the reason why we did not observe strong segmental defects. Gene reporter activity was also observed in other lineages, including parts of the neural tube and the intermediate mesoderm. Therefore, although a detailed lineage study will be required in future studies, the activity that we observed in our *CAG-CAT-Mesp2/Mox1-Cre* transgenics proved to be useful for the manipulation of gene expression, at least in the somitic cell lineages. Recently, a similar Cre line (*Meox1*^{cre}) was reported by another laboratory and the results of their study were consistent with our current data (Jukkola et al., 2005).

We are grateful to Dr Baljinder S. Mankoo for generously providing the genomic DNA clones for *Mox1* and Drs Alan Rawls, Sachiko Iseki and Atsuko Sehara for cDNA clones encoding paraxis, twist and *Myod1*, respectively. We also thank Masayuki Oginuma and Dr Kenta Sumiyama for advice on the transgenic mouse analysis. This work was supported by Grants-in-Aid for Science Research on Priority Areas (B), the Organized Research Combination System and National BioResource Project of the Ministry of Education, Culture, Sports, Science and Technology, Japan.

Supplementary material

Supplementary material for this article is available at http://dev.biologists.org/cgi/content/full/133/13/2517/DC1

References

Akiyama, H., Kamitani, T., Yang, X., Kandyil, R., Bridgewater, L. C., Fellous, M., Mori-Akiyama, Y. and de Crombrugghe, B. (2005). The transcription factor Sox9 is degraded by the ubiquitin-proteasome system and stabilized by a mutation in a ubiquitin-target site. *Matrix Biol.* **23**, 499-505.

Aulehla, A. and Herrmann, B. (2004). Segmentation in vertebrates: clock and gradient finally joined. *Genes Dev.* **18**, 2060-2067.

Barrios, A., Poole, R. J., Durbin, L., Brennan, C., Holder, N. and Wilson, S. W. (2003). Eph/Ephrin signaling regulates the mesenchymal-to-epithelial transition of the paraxial mesoderm during somite morphogenesis. *Curr. Biol.* **13**, 1571-1582.

Bessho, Y. and Kageyama, R. (2003). Oscillations, clocks and segmentation. *Curr. Opin. Genet. Dev.* **13**, 379-384.

Bussen, M., Petry, M., Schuster-Gossler, K., Leitges, M., Gossler, A. and Kispert, A. (2004). The T-box transcription factor Tbx18 maintains the separation of anterior and posterior somite compartments. *Genes Dev.* **18**, 1209-1221.

Cooke, J., Kemp, H. and Moens, C. (2005). EphA4 is required for cell adhesion and rhombomere-boundary formation in the zebrafish. *Curr. Biol.* **15**, 536-542.

Denetclaw, W. F. and Ordahl, C. P. (2000). The growth of the dermomyotome and formation of early myotome lineages in thoracolumbar somites of chicken embryos. *Development* **127**, 893-905.

Dottori, M., Hartley, L., Galea, M., Paxinos, G., Polizzotto, M., Kilpatrick, T., Bartlett, P. F., Murphy, M., Kontgen, F. and Boyd, A. W. (1998). EphA4 (Sek1) receptor tyrosine kinase is required for the development of the corticospinal tract. *Proc. Natl. Acad. Sci. USA* **95**, 13248-13253.

Durbin, L., Brennan, C., Shiomi, K., Cooke, J., Barrios, A., Shanmugalingam, S., Guthrie, B., Lindberg, R. and Holder, N. (1998). Eph signaling is required for segmentation and differentiation of the somites. *Genes Dev.* **12**, 3096-3109.

Imai, Y., Matsushima, Y., Sugimura, T. and Terada, M. (1991). A simple and rapid method for generating a deletion by PCR. *Nucleic Acids Res.* **19**, 2785.

Jukkola, T., Trokovic, R., Maj, P., Lamberg, A., Mankoo, B., Pachnis, V., Savilahti, H. and Partanen, J. (2005). Meox1Cre: a mouse line expressing Cre recombinase in somitic mesoderm. *Genesis* **43**, 148-153.

Kothary, R., Clapoff, S., Darling, S., Perry, M., Moran, L. and Rossant, J. (1989). Inducible expression of an hsp68-lacZ hybrid gene in transgenic mice. *Development* **105**, 707-714.

Kullander, K., Mather, N. K., Diella, F., Dottori, M., Boyd, A. W. and Klein, R. (2001). Kinase-dependent and kinase-independent functions of EphA4 receptors in major axon tract formation in vivo. *Neuron* **29**, 73-84.

Ledent, V. and Vervoort, M. (2001). The basic helix-loop-helix protein family: comparative genomics and phylogenetic analysis. *Genome Res.* **11**, 754-770.

Leitges, M., Neidhardt, L., Haenig, B., Herrmann, B. and Kispert, A. (2000). The paired homeobox gene Uncx4.1 specifies pedicles, transverse processes and proximal ribs of the vertebral column. *Development* **127**, 2259-2267.

Lluis, F., Ballestar, E., Suelves, M., Esteller, M. and Munoz-Canoves, P. (2005).

E47 phosphorylation by p38 MAPK promotes MyoD/E47 association and muscle-specific gene transcription. *EMBO J.* **24**, 974-984.
Mankoo, B., Skuntz, S., Harrigan, I., Grigorieva, E., Candia, A., Wright, C., Arnheiter, H. and Pachnis, V. (2003). The concerted action of Meox homeobox genes is required upstream of genetic pathways essential for the formation, patterning and differentiation of somites. *Development* **130**, 4655-4664.
Mansouri, A., Voss, A., Thomas, T., Yokota, Y. and Gruss, P. (2000). Uncx4.1 is required for the formation of the pedicles and proximal ribs and acts upstream of Pax9. *Development* **127**, 2251-2258.
Maroto, M. and Pourquié, O. (2001). A molecular clock involved in somite segmentation. *Curr. Top. Dev. Biol.* **51**, 221-248.
Morimoto, M., Takahashi, Y., Endo, M. and Saga, Y. (2005). The Mesp2 transcription factor establishes segmental borders by suppressing Notch activity. *Nature* **435**, 354-359.
Nakaya, Y., Kuroda, S., Katagiri, Y., Kaibuchi, K. and Takahashi, Y. (2004). Mesenchymal-epithelial transition during somitic segmentation is regulated by differential roles of Cdc42 and Rac1. *Dev. Cell* **7**, 425-438.
Nomura-Kitabayashi, A., Takahashi, Y., Kitajima, S., Inoue, T., Takeda, H. and Saga, Y. (2002). Hypomorphic Mesp allele distinguishes establishment of rostrocaudal polarity and segment border formation in somitogenesis. *Development* **129**, 2473-2481.
Perini, G., Diolaiti, D., Porro, A. and Della Valle, G. (2005). In vivo transcriptional regulation of N-Myc target genes is controlled by E-box methylation. *Proc. Natl. Acad. Sci. USA* **102**, 12117-12122.
Pourquié, O. (2003). The segmentation clock: converting embryonic time into spatial pattern. *Science* **301**, 328-330.
Powell, L. M., Zur Lage, P. I., Prentice, D. R., Senthinathan, B. and Jarman, A. P. (2004). The proneural proteins Atonal and Scute regulate neural target genes through different E-box binding sites. *Mol. Cell. Biol.* **24**, 9517-9526.
Rida, P., Le Minh, N. and Jiang, Y. (2004). A Notch feeling of somite segmentation and beyond. *Dev. Biol.* **265**, 2-22.
Saga, Y. and Takeda, H. (2001). Mesp2: a novel mouse gene expressed in the presegmented mesoderm and essential for segmentation initiation. *Nat. Rev. Genet.* **11**, 835-845.
Saga, Y., Hata, N., Koseki, H. and Taketo, M. M. (1997). Mesp2: a novel mouse gene expressed in the presegmented mesoderm and essential for segmentation initiation. *Genes Dev.* **11**, 1827-1839.
Saga, Y., Miyagawa-Tomita, S., Takagi, A., Kitajima, S., Miyazaki, J. and Inoue, T. (1999). MesP1 is expressed in the heart precursor cells and required for the formation of a single heart tube. *Development* **126**, 3437-3447.
Sakai, K. and Miyazaki, J. (1997). A transgenic mouse line that retains Cre recombinase activity in mature oocytes irrespective of the cre transgene transmission. *Biochem. Biophys. Res. Commun.* **237**, 318-324.
Takahashi, Y., Koizumi, K., Takagi, A., Kitajima, S., Inoue, T., Koseki, H. and Saga, Y. (2000). Mesp2 initiates somite segmentation through the Notch signalling pathway. *Nat. Genet.* **25**, 390-396.
Theil, T., Frain, M., Gilardi-Hebenstreit, P., Flenniken, A., Charnay, P. and Wilkinson, D. (1998). Segmental expression of the EphA4 (Sek-1) receptor tyrosine kinase in the hindbrain is under direct transcriptional control of Krox-20. *Development* **125**, 443-452.
Yamauchi, Y., Abe, K., Mantani, A., Hitoshi, Y., Suzuki, M., Osuzu, F., Kuratani, S. and Yamamura, K. (1999). A novel transgenic technique that allows specific marking of the neural crest cell lineage in mice. *Dev. Biol.* **212**, 191-203.
Zambrowicz, B., Imamoto, A., Fiering, S., Herzenberg, L., Kerr, W. and Soriano, P. (1997). Disruption of overlapping transcripts in the ROSA beta geo 26 gene trap strain leads to widespread expression of beta-galactosidase in mouse embryos and hematopoietic cells. *Proc. Natl. Acad. Sci. USA* **94**, 3789-3794.

Available online at www.sciencedirect.com
ScienceDirect
Biochemical and Biophysical Research Communications 354 (2007) 892–898
BBRC
www.elsevier.com/locate/ybbrc

Functional characterization of a new p53 mutant generated by homozygous deletion in a neuroblastoma cell line

Yohko Nakamura [1], Toshinori Ozaki [1], Hidetaka Niizuma, Miki Ohira, Takehiko Kamijo, Akira Nakagawara *

Division of Biochemistry, Chiba Cancer Center Research Institute, Chiba 260-8717, Japan

Received 11 January 2007
Available online 22 January 2007

Abstract

p53 is a key modulator of a variety of cellular stresses. In human neuroblastomas, p53 is rarely mutated and aberrantly expressed in cytoplasm. In this study, we have identified a novel p53 mutant lacking its COOH-terminal region in neuroblastoma SK-N-AS cells. p53 accumulated in response to cisplatin (CDDP) and thereby promoting apoptosis in neuroblastoma SH-SY5Y cells bearing wild-type *p53*, whereas SK-N-AS cells did not undergo apoptosis. We found another p53 (p53ΔC) lacking a part of oligomerization domain and nuclear localization signals in SK-N-AS cells. p53ΔC was expressed largely in cytoplasm and lost the transactivation function. Furthermore, a 3′-part of the *p53* locus was homozygously deleted in SK-N-AS cells. Thus, our present findings suggest that p53 plays an important role in the DNA-damage response in certain neuroblastoma cells and it seems to be important to search for *p53* mutations outside DNA-binding domain.

Keywords: Apoptosis; Cisplatin; Homozygous deletion; Neuroblastoma; p53

p53 plays a pivotal role in the regulation of cell cycle arrest and apoptosis. *p53* is one of the most frequently mutated genes in human tumors [1,2] and *p53*-deficient mice developed spontaneous tumors [3]. Upon a variety of cellular stresses, p53 accumulates in nucleus through post-translational modifications including phosphorylation and acetylation and thereby exerting its function [4]. Pro-apoptotic function of p53 is closely linked to its DNA-binding activity. p53 acts as a transcription factor to transactivate a variety of its target genes. Indeed, 95% of *p53* mutations in human tumors occur within its DNA-binding region and these mutations inactivate pro-apoptotic function of p53 [4].

Alternatively, p53 is inhibited by various mechanisms. MDM2 acts as an E3 ubiquitin ligase for p53 and promotes its proteolytic degradation through ubiquitin–proteasome pathway [5,6]. Subcellular distribution of p53 also plays a key role in the regulation of p53 [4]. p53 contains three nuclear localization signals (NLS I, II, and III) in its COOH-terminal region [7,8]. In contrast to other human tumors, *p53* is rarely mutated in neuroblastomas [9]. Neuroblastoma cells showed a cytoplasmic localization of wild-type p53 and exhibited an impaired p53-mediated cell cycle arrest in response to DNA damage, suggesting that there exists a mutation-independent mechanism of p53 inactivation [10–12]. Intriguingly, Nikolaev et al. demonstrated that Parkin-like ubiquitin ligase termed Parc serves as an anchor protein that tethers p53 in cytoplasm and thereby regulating subcellular localization and function of p53 [13].

In this study, we have identified a novel p53 mutant (p53ΔC) homozygously deleted in neuroblastoma SK-N-AS cells and our current studies suggest that *p53* status plays an important role in the cell fate determination of certain neuroblastoma cells in response to DNA damage.

* Corresponding author. Fax: +81 43 265 4459.
E-mail address: akiranak@chiba-cc.jp (A. Nakagawara).
[1] These authors contributed equally to this work.

0006-291X/$ - see front matter © 2007 Elsevier Inc. All rights reserved.
doi:10.1016/j.bbrc.2007.01.057

Materials and methods

Cell culture and transfection. Neuroblastoma cells were grown in RPMI 1640 medium supplemented with 10% heat-inactivated fetal bovine serum (FBS, Invitrogen) and antibiotic mixture in a humidified atmosphere of 5% CO_2 in air at 37 °C. For transfection, cells were transfected with the indicated expression plasmids using LipofectAMINE 2000 according to the manufacturer's instructions (Invitrogen).

Construction of p53 mutant. cDNA encoding p53 mutant was amplified by PCR using cDNA from SK-N-AS cells. Forward and reverse primers were 5′-AATATTTCACCCTTCAGGTACTAAG-3′ (forward) and 5′-CTCGAGTCACTGCCCCCTGATGGC-3′ (reverse). *Ssp*I and *Xho*I sites shown in boldface type were introduced into forward and reverse primers, respectively. PCR products were gel-purified and subcloned into pGEM-T plasmid (Promega). Constructs were confirmed by sequencing and then digested with *Ssp*I and *Xho*I. The digested fragment was again gel-purified and then ligated with the *Ssp*I and *Bam*HI fragment of FLAG-p53 to give pcDNA3-FLAG-p53CΔ.

RNA preparation and RT-PCR analysis. Total RNA was prepared using RNeasy Mini kit (Qiagen) following the manufacturer's protocol. cDNA was synthesized using SuperScript II with random primers (Invitrogen) and amplified by PCR using primers as described: *p53*: forward, 5′-CTGCCCTCAACAAGATGTTTTG-3′, and reverse, 5′-CTATCTGAGCAGCGCTCATGG-3′; *p21*^{WAF1}: forward, 5′-ATGAAATTCACCCCCTTTCC-3′, and reverse, 5′-CCCTAGGCTGTGCTCACTTC-3′; *Bax*: forward, 5′-TTTGCTTCAGGGTTTCATCC-3′, and reverse, 5′-CAGTTGAAGTTGCCGTCAGA-3′; *p53AIP1*: forward, 5′-CCAAGTTCTCTGCTTTC-3′ and reverse, 5′-AGCTGAGCTCAAATGCTGAC-3′; *PUMA*: forward, 5′-TATGGATCCCGCACCATGGACTACAAGGACGACGATGACAAGGCCCGCGCACGCCAG-3′ and reverse, 5′-TATGGATCCCTACATGGTGCAGAGAAAGTCCCCC-3′; and *GAPDH*: forward, 5′-ACCTGACCTGCCGTCTAGAA-3′, and reverse, 5′-TCCACCACCCTGTTGCTGTA-3′.

Southern blotting. Genomic DNA was digested with *Pst*I, separated by 1% agarose gel electrophoresis, and transferred onto nylon membranes. Hybridization was performed at 65 °C in a solution containing 1 M NaCl, 1% *N*-lauroyl sarcosine, 7.5% dextran sulfate, 100 μg of heat-denatured salmon sperm DNA/ml, and radio-labeled DNA. After hybridization, membranes were washed twice with 2× SSC/0.1% *N*-lauroyl sarcosine at 50 °C and exposed to an X-ray film at −70 °C.

Immunoblotting. Cells were lysed in lysis buffer containing 25 mM Tris–HCl, pH 8.0, 137 mM NaCl, 2.7 mM KCl, 1% Triton X-100, and protease inhibitor mixture (Sigma). Lysates were separated by SDS–PAGE and transferred onto Immobilon-P membranes (Millipore). Membranes were probed with anti-p53 (DO-1, Calbiochem), anti-p53 (PAb122, BD Pharmingen), anti-phosphorylated p53 at Ser-15 (Cell Signaling) or with anti-actin (20–33, Sigma) followed by incubation with HRP-conjugated goat anti-mouse or anti-rabbit IgG secondary antibody (Cell Signaling). Immunoreactive bands were detected using chemiluminescence (ECL, Amersham Biosciences).

Subcellular fractionation. Cells were lysed in lysis buffer containing 10 mM Tris–HCl, pH 7.5, 1 mM EDTA, 0.5% NP-40, and protease inhibitor mixture (Sigma). Lysates were centrifuged to separate soluble (cytosolic) from insoluble (nuclear) fractions. The nuclear and cytosolic fractions were subjected to immunoblotting using anti-p53, anti-Lamin B (Ab-1, Oncogene Research products) or with anti-tubulin-α (Ab-2, NeoMarkers).

Array-based comparative genomic hybridization (CGH) analysis. Whole genome arrays of 2464 bacterial artificial chromosome (BAC) clones were hybridized simultaneously with 500 ng of target DNA (SK-N-AS, RTBM1, and SH-SY5Y) and reference DNA (normal female genomic DNA). Target DNAs were labeled with Cy3-dCTP and reference DNAs with Cy5-dCTP by random priming. Hybridization, scanning, and data processing were conducted as described previously [14,15].

Cell survival assays. Cells were plated at a density of 5000 cells/well in 96-well tissue culture plates. After attachment overnight, medium was replaced and treated with CDDP for 24 h. Cell viability was measured by MTT assay.

Flow cytometry. Floating and adherent cells were pooled and fixed in ice-cold 70% ethanol for 4 h at −20 °C. Cells were then stained with 10 mg/ml of PI (Sigma) in the presence of 250 mg/ml of RNase A at 37 °C for 30 min in the dark. Number of cells with sub-G1 DNA content was measured by flow cytometry (FACScan, Becton–Dickinson).

TUNEL assay. Apoptotic cells were identified using an *in situ* cell detection, peroxidase kit (Roche Applied Science). Briefly, cells were fixed in 4% paraformaldehyde and permeabilized with 0.1% Triton X-100. The labeling reaction was performed using TMR red-labeled dUTP together with other nucleotides by terminal deoxynucleotidyl transferase for 1 h in the dark at 37 °C. Then, cells were mounted and the incorporated TMR red-labeled dUTP was analyzed using a Fluoview laser scanning confocal microscope (Olympus).

Luciferase reporter assay. H1299 cells were co-transfected with pcDNA3, FLAG-p53 or FLAG-p53ΔC expression plasmid, p53-responsive luciferase reporter (*p21*^{WAF1}, *MDM2* or *Bax*), and pRL-TK *Renilla* luciferase cDNA. Forty-eight hours after transfection, firefly and *Renilla* luciferase activities were measured with dual-luciferase reporter assay system according to the manufacturer's instructions (Promega).

Colony formation assay. Forty-eight hours after transfection, SK-N-AS cells were transferred to fresh medium containing G418 (400 μg/ml). After 16 days of selection, drug-resistant colonies were fixed in methanol and stained with Giemsa's solution.

Results

DNA-damage response in human neuroblastoma cells

To determine the effects of genotoxic agents on neuroblastomas, human neuroblastoma SH-SY5Y and SK-N-AS cells were exposed to cisplatin (CDDP) and their viabilities were examined by MTT assays. As shown in Fig. 1A, their viabilities were significantly decreased in response to CDDP. To address whether CDDP could induce apoptosis, we performed TUNEL assay. As shown in Fig. 1B, we observed a higher number of TUNEL-positive SH-SY5Y cells exposed to CDDP, whereas CDDP had undetectable effects on SK-N-AS cells. We further determined apoptotic cells as sub-G1 population by flow cytometry. As seen in Fig. 1C, a significant increase in number of SH-SY5Y cells with sub-G1 DNA content was observed after CDDP treatment, whereas CDDP treatment of SK-N-AS cells resulted in an increase in S-phase cells but not in G2/M-phase cells. Consistent with these results, *thymidine kinase* (S-phase marker) [16] was increased in CDDP-treated SK-N-AS cells, whereas *Plk1* (M-phase marker) [17] remained unchanged regardless of CDDP treatment (data not shown).

We then examined whether p53-dependent apoptotic pathway could be activated in response to CDDP. As shown in Fig. 1D, p53 was phosphorylated at Ser-15 in SH-SY5Y cells exposed to CDDP. *p53* remained unchanged regardless of CDDP treatment, whereas p53 target genes including *p21*^{WAF1}, *Bax*, and *PUMA* were transactivated in response to CDDP. In contrast, CDDP-mediated phosphorylation of p53 at Ser-15 was undetectable in SK-N-AS cells. *p21*^{WAF1} was induced in response to CDDP, however, CDDP-mediated up-regulation of pro-apoptotic *Bax* and *PUMA* was undetectable, suggesting that p53 pro-apoptotic function might be lost in SK-N-AS cells.

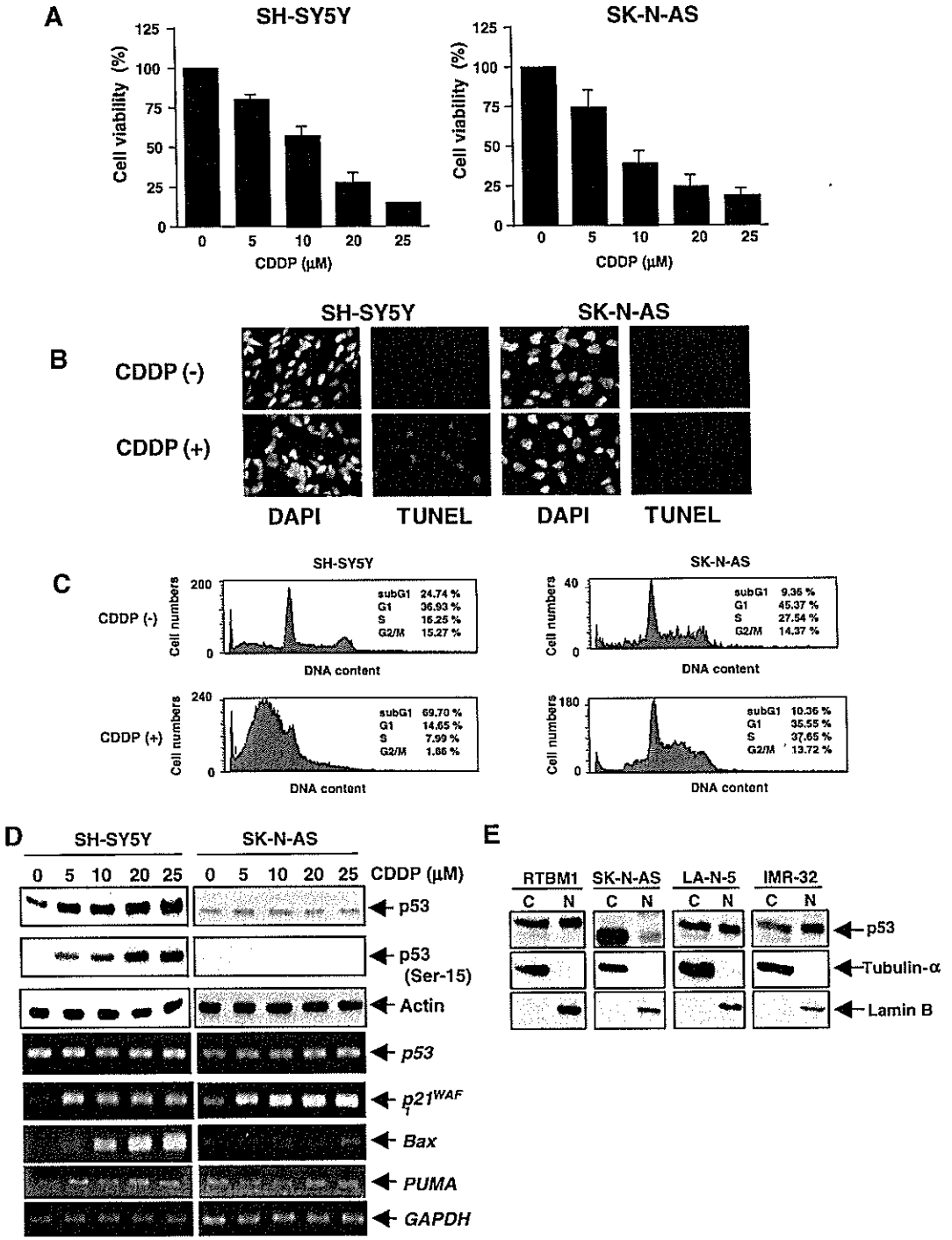

Fig. 1. Differential effects of CDDP on neuroblastoma cells. (A) Cell survival assays. Twenty-four hours after CDDP treatment, cell viability was analyzed by MTT assays. (B) TUNEL staining. Twenty-four hours after CDDP treatment (20 μM), apoptotic cells were detected by TUNEL staining. Cell nuclei were stained with DAPI. (C) FACS analysis. SH-SY5Y and SK-N-AS cells were treated as in (B). Twenty-four hours after CDDP treatment, cell cycle distributions were analyzed by FACS. Shown are the representatives of three independent experiments. (D) CDDP-induced accumulation of p53 in neuroblastoma cells. Twenty-four hours after CDDP treatment, lysates and total RNA were subjected to immunoblotting (upper panels) and RT-PCR (lower panels), respectively. For protein loading control, actin levels were checked by immunoblotting. For RT-PCR, *GAPDH* was used as a loading control. (E) Subcellular localization of p53. The indicated neuroblastoma cells were fractionated into cytoplasmic (C) and nuclear (N) fractions and subcellular distribution of p53 was analyzed by immunoblotting. Tubulin-α and Lamin B were used as cytoplasmic and nuclear markers, respectively.

To investigate molecular mechanism(s) behind p53 dysfunction in SK-N-AS cells, we examined subcellular localization of p53 in various neuroblastoma cells. As shown in Fig. 1E, p53 was detected in cytoplasm and nucleus of RTBM1, LA-N-5, and IMR-32 cells bearing wild-type *p53* (data not shown). Of note, p53 was abundantly expressed in cytoplasm of SK-N-AS cells and its molecular mass was smaller than those of other

cells, indicating that it might be due to certain structural aberrations.

Structural aberration of p53 in SK-N-AS cells

To address whether p53 could have any aberrations in SK-N-AS cells, we amplified the indicated genomic regions of *p53* using genomic DNA from SK-N-AS cells. RTBM1 cells were used as a positive control. As shown in Fig. 2A, PCR-based amplification using primer sets including P1, P2, P6, and P7 successfully generated estimated sizes of PCR products, whereas remaining primer sets (P3–P5) did not, suggesting that the genomic region containing exons 10 and 11 of *p53* might be lost in SK-N-AS cells.

To confirm genomic aberrations within *p53* locus in SK-N-AS cells, we performed Southern analysis. Radio-labeled *p53* cDNA probe failed to detect *Pst*I fragment (2.0 kb in length) which contains exons 10 and 11 in SK-N-AS cells (Fig. 2B). Our array-based comparative genomic hybridization (CGH) analysis demonstrated that there exists a large range of allelic deletion of chromosome 17p where *p53* is located in SK-N-AS cells (Fig. 2C). Furthermore, anti-p53 antibody which recognizes p53 extreme COOH-terminal portion could not detect p53 in SK-N-AS cells (Fig. 2D). Collectively, our results suggest that p53 COOH-terminal region is homozygously deleted in SK-N-AS cells. We then cloned *p53* cDNA. As shown in Fig. 2E, a newly identified p53 (p53ΔC) was composed of 369 amino acids including unique COOH-terminal structure (estimated molecular mass of 49 kDa), lacked a part of oligomerization domain, and completely lost NLS II and III. The 3′-side of intron 9 and the downstream region containing exons 10 and 11 were deleted in SK-N-AS cells. Its unique COOH-terminal amino acids were derived from intron 9, suggesting that accurate splicing event might be abrogated and thereby generating p53ΔC.

Dysfunction of p53ΔC

To ask whether p53ΔC could have functional differences as compared with wild-type p53, FLAG-p53 or FLAG-p53ΔC was expressed in SK-N-AS cells and their subcellular localization was examined. As shown in Fig. 3A, FLAG-p53 was detectable in cytoplasm and nucleus,

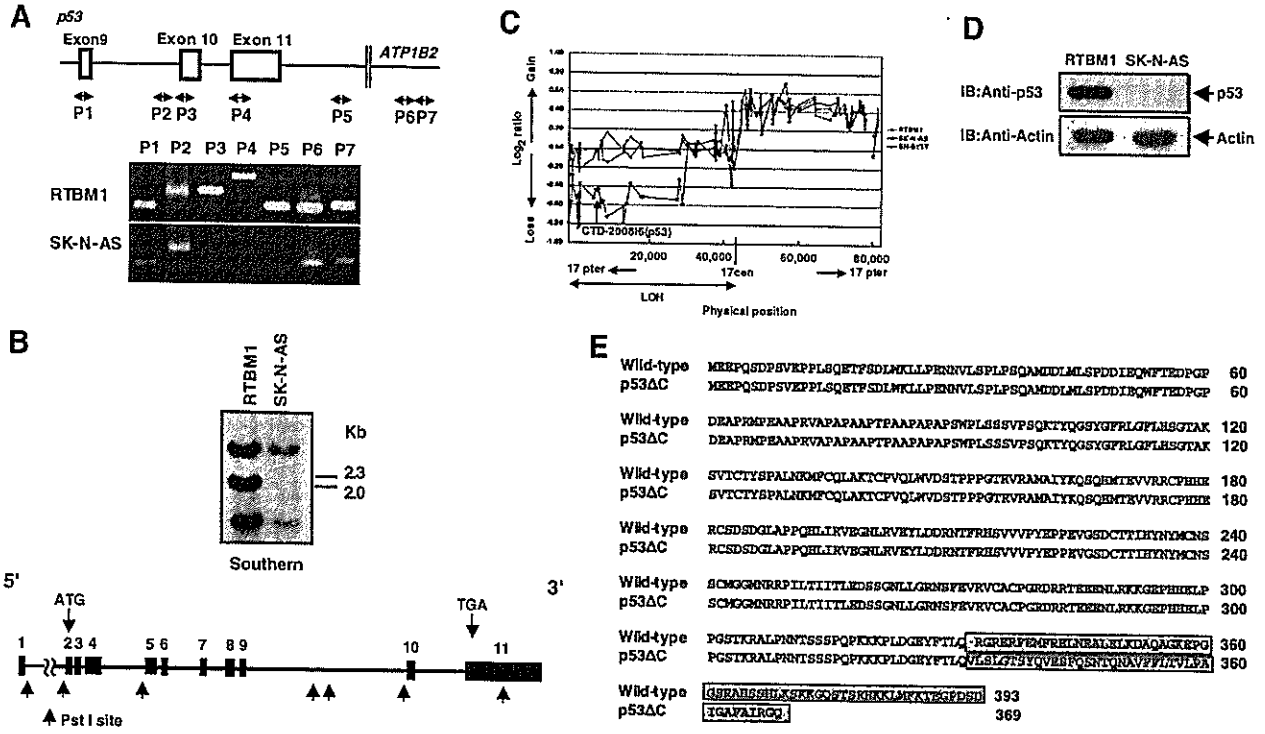

Fig. 2. p53 COOH-terminal region is deleted in SK-N-AS cells. (A) Genomic structure of human *p53* locus and positions of PCR primers (P1–P7) are shown. *ATP1B2* encodes ATPase, Na^+/K^+ transporting β2 (upper panel). Genomic DNA from RTBM1 and SK-N-AS cells was subjected to PCR using the indicated primers (lower panels). (B) Southern blot analysis. Genomic DNA was digested with *Pst*I, separated by 1% agarose gel, transferred onto nylon membrane, and probed with the radio-labeled *p53* cDNA. Schematic diagram of human *p53* and positions of *Pst*I sites are also shown. (C) Array-based comparative genomic hybridization (CGH) analysis. Hybridization was performed as described under Materials and methods. Arrays were scanned and images processed using custom software. We normalized relative ratios of tumor and normal signals by setting the value of the median relative ratio equal to 1. The data were then transformed into log 2 space and plotted as a histogram to determine cutoffs for scoring loss or gain. Three Gaussian distribution curves were fitted to the histogram, and values >3 SD from the central Gaussian were scored as losses or gains for that tumor. (D) Immunoblotting. Lysates from RTBM1 and SK-N-AS were processed for immunoblotting with the specific antibody against p53 extreme COOH-terminal portion. (E) Amino acid sequence alignment of wild-type p53 and p53ΔC. The different amino acid residues between them are boxed.

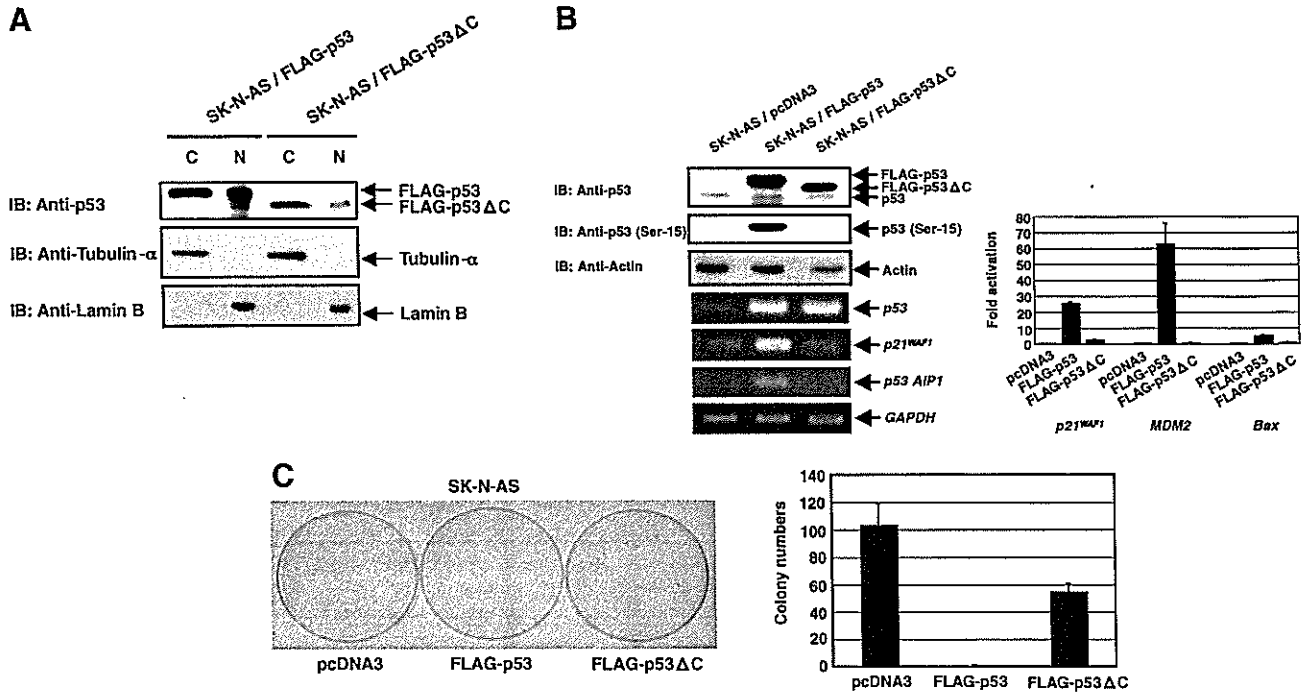

Fig. 3. Loss of function of p53ΔC. (A) Subcellular localization of exogenously expressed wild-type p53 and p53ΔC. SK-N-AS cells were transfected with the indicated expression plasmids. Forty-eight hours after transfection, cells were fractionated into cytoplasmic (C) and nuclear (N) fractions followed by immunoblotting with anti-p53 antibody. (B) Possible effects of COOH-terminal deletion of p53 on its transcriptional activity. SK-N-AS cells were transfected with the indicated expression plasmids. Forty-eight hours after transfection, lysates and total RNA were subjected to immunoblotting and RT-PCR, respectively (left panel). (Right panel) Luciferase reporter assays. *p53*-deficient H1299 cells were co-transfected with pcDNA3, FLAG-p53 or FLAG-p53ΔC expression plasmid, p53-responsive luciferase reporter (*$p21^{WAF1}$*, *MDM2* or *Bax*) and *Renilla* luciferase cDNA. Forty-eight hours after transfection, luciferase activities were measured. (C) Colony formation assay. Forty-eight hours after transfection, SK-N-AS cells were transferred to fresh medium containing G418 (400 μg/ml). Sixteen days after selection with G418, drug-resistant colonies were stained with Giemsa's solution (left panel) and the number of colonies was scored (right panel).

whereas FLAG-p53ΔC was largely expressed in cytoplasm. Next, we examined transcriptional potential of p53ΔC in SK-N-AS cells. As seen in left panel of Fig. 3B, FLAG-p53 but not FLAG-p53ΔC was phosphorylated at Ser-15. Consistent with these results, FLAG-p53 transactivated *$p21^{WAF1}$* and *p53AIP1*. In contrast, FLAG-p53ΔC failed to transactivate *$p21^{WAF1}$* and *p53AIP1*. Similar results were also obtained by luciferase reporter assays (Fig. 3B, right panel). To examine effects of COOH-terminal deletion on pro-apoptotic activity of p53, we performed colony formation assays. SK-N-AS cells were transfected with empty plasmid, FLAG-p53 or FLAG-p53ΔC expression plasmid and maintained in medium containing G418 for 16 days. As shown in Fig. 3C, number of drug-resistant colonies was significantly reduced in cells expressing FLAG-p53. Intriguingly, enforced expression of FLAG-p53ΔC resulted in a decrease in number of drug-resistant colonies but to a lesser degree as compared with that in cells expressing FLAG-p53. These observations suggest that COOH-terminal deletion reduces transcriptional and pro-apoptotic activities of p53.

Discussion

In this study, we have identified p53ΔC in SK-N-AS cells. Consistent with the recent report [13], p53 was predominantly expressed in cytoplasm of SK-N-AS cells. According to their results, Parc inhibited p53 nuclear translocation through the direct interaction with its COOH-terminal region. Since p53 contains three NLSs in its COOH-terminal region, Parc might inhibit its nuclear access by masking its NLSs [13]. In accordance with these findings, p53 COOH-terminal peptide inhibited its cytoplasmic retention [12]. Based on our immunoprecipitation experiments, wild-type p53 but not p53ΔC was co-immunoprecipitated with the endogenous Parc in SK-N-AS cells (data not shown), suggesting that cytoplasmic retention of p53ΔC is regulated in a Parc-independent manner. p53ΔC lacks NLS II and III but retains NLS I. Although Kim et al. described that importin-α interacts with NLS I of p53 and mediates its nuclear import [18], NLS II and/or III might play a major role in nuclear import of p53 in SK-N-AS cells.

p53 phosphorylation is significantly associated with its pro-apoptotic function [4]. Exogenously expressed wild-type p53 but not p53ΔC was phosphorylated at Ser-15 in SK-N-AS cells without DNA damage and transactivated *$p21^{WAF1}$* and *p53AIP1*. Rodicker and Putzer described that exogenously expressed p53 is phosphorylated at Ser-15 without DNA damage [19]. Although it is unknown why exogenously expressed p53 but not p53ΔC is phosphorylated at Ser15 without DNA damage, it might be at least

in part due to its cytoplasmic retention. Colony formation assays demonstrated that wild-type p53 markedly reduces number of drug-resistant colonies in SK-N-AS cells, suggesting that there might not exist functional disruptions of downstream mediators of p53 in SK-N-AS cells. In response to CDDP, SH-SY5Y cells underwent apoptosis in association with a significant induction of p53. On the other hand, SK-N-AS cells did not undergo apoptosis in response to CDDP, suggesting that *p53* status might determine neuroblastoma cell fate to survive or to die. Intriguingly, CDDP treatment of SK-N-AS cells induced an accumulation of S-phase cells accompanied with up-regulation of $p21^{WAF1}$. Since p53ΔC failed to transactivate $p21^{WAF1}$ and CDDP had undetectable effects on *p73* and *p63* (other members of *p53* family) (data not shown), CDDP-mediated up-regulation of $p21^{WAF1}$ in SK-N-AS cells is regulated in a p53 family-independent manner. Knudsen et al. reported that CDDP-mediated DNA damage induces an intra-S-phase cell cycle arrest, which is correlated with a protection against apoptosis [20]. Thus, the genome maintenance system might delay the onset of mitosis, and thereby providing time to complete DNA repair and/or DNA replication before cell division in SK-N-AS cells. Further efforts should be necessary to address this issue.

Majority of *p53* mutations is detected within its DNA-binding region [21]. SK-N-AS cells have been believed to express wild-type p53 [22]. Much of information regarding *p53* mutations was derived from sequence analysis of exons 5–8 which encode its DNA-binding domain [4]. Indeed, there exist missense mutations in p53 oligomerization domain [23]. According to their results, Leu to Pro substitution at 344 inhibited the oligomerization of p53 and abolished its DNA-binding activity. Since p53ΔC lacks a part of oligomerization domain including Leu-344, p53ΔC might exist as a monomeric latent form. Recently, Bourdon et al. described that human *p53* is expressed as multiple isoforms including p53β and p53γ [24]. Based on amino acid sequence comparison, p53ΔC was distinct from p53β and p53γ (data not shown). During the preparation of our manuscript, Goldschneider et al. reported that SK-N-AS cells express p53β [25]. This discrepancy might be attributed to co-expression of p53β and p53ΔC in SK-N-AS cells and/or due to the acquired heterogeneity of SK-N-AS cells during culture. Additionally, murine *p53* expresses an alternative splicing isoform termed ASp53 with different COOH-terminus from that of wild-type p53 [26]. ASp53 displays an enhanced transcriptional activity as compared with wild-type p53, indicating that p53ΔC is distinct from human counterpart of ASp53.

Acknowledgments

This work was supported in part by a Grant-in-Aid from the Ministry of Health, Labor and Welfare for Third Term Comprehensive Control Research for Cancer, a Grant-in-Aid for Scientific Research on Priority Areas from the Ministry of Education, Culture, Sports, Science and Technology, Japan, a Grant-in-Aid for Scientific Research from Japan Society for the Promotion of Science, and a Grant from Uehara Memorial Foundation.

References

[1] M. Hollstein, D. Sidransky, B. Vogelstein, H. Harris, p53 mutations in human cancers, Science 253 (1991) 49–53.
[2] A.J. Levine, J. Momand, C.A. Finlay, The p53 tumour suppressor gene, Nature 351 (1991) 453–456.
[3] L.A. Donehower, M. Harvey, B.L. Slagle, M.J. McArthur, C.A. Montgomery Jr., J.S. Butel, A. Bradley, Mice deficient for p53 are developmentally normal but susceptible to spontaneous tumours, Nature 356 (1992) 215–221.
[4] K.H. Vousden, X. Lu, Live or let die: the cells response to p53, Nat. Rev. Cancer 2 (2002) 594–604.
[5] Y. Haupt, R. Maya, A. Kazaz, M. Oren, Mdm2 promotes the rapid degradation of p53, Nature 387 (1997) 296–299.
[6] M.H.G. Kubbutat, S.N. Jones, K.H. Vousden, Regulation of p53 stability by Mdm2, Nature 387 (1997) 299–303.
[7] G. Shaulsky, N. Goldfinger, A. Ben-Ze'ev, V. Rotter, Nuclear accumulation of p53 protein is mediated by several nuclear localization signals and plays a role in tumorigenesis, Mol. Cell. Biol. 10 (1990) 6565–6577.
[8] S.H. Liang, D. Hong, M.F. Clarke, Cooperation of a single lysine mutation and a C-terminal domain in the cytoplasmic sequestration of the p53 protein, J. Biol. Chem. 273 (1998) 19817–19821.
[9] K. Vogan, M. Bernstein, J.M. Leclerc, L. Brisson, J. Brossard, G.M. Brodeur, J. Pelletier, P. Gros, Absence of p53 gene mutations in primary neuroblastomas, Cancer Res. 53 (1993) 5269–5273.
[10] U.M. Moll, M. LaQuaglia, J. Benard, G. Riou, Wild-type p53 protein undergoes cytoplasmic sequestration in undifferentiated neuroblastomas but not in differentiated tumors, Proc. Natl. Acad. Sci. USA 92 (1995) 4407–4411.
[11] U.M. Moll, A.G. Ostermeyer, R. Haladay, B. Winkfield, M. Frazier, G. Zambetti, Cytoplasmic sequestration of wild-type p53 protein impairs the G1 checkpoint after DNA damage, Mol. Cell. Biol. 16 (1996) 1126–1137.
[12] A.G. Ostermeyer, E. Runko, B. Winkfield, B. Ahn, U.M. Moll, Cytoplasmically sequestrated wild-type p53 protein in neuroblastoma is relocated to the nucleus by a C-terminal peptide, Proc. Natl. Acad. Sci. USA 93 (1996) 15190–15194.
[13] A.Y. Nikolaev, M. Li, N. Puskas, J. Qin, W. Gu, Parc: A cytoplasmic anchor for p53, Cell 112 (2003) 29–40.
[14] A.M. Snijders, N. Nowak, R. Segraves, S. Blackwood, N. Brown, J. Conroy, G. Hamilton, A.K. Hindle, B. Huey, K. Kimura, S. Law, K. Myambo, J. Palmer, B. Yistra, J.P. Yue, J.W. Gray, A.N. Jain, D. Pinkel, D.G. Albertson, Assembly of microarrays for genome-wide measurement of DNA copy number, Nat. Genet. 29 (2001) 263–264.
[15] J.M. Nigro, A. Misra, L. Zhang, I. Smimov, H. Colman, C. Griffin, N. Ozburn, M. Chen, E. Pan, D. Koul, W.K. Yung, B.G. Feuerstein, K.D. Aldape, Integrated array-comparative genomic hybridization and expression array profiles identity clinically relevant molecular subtypes of glioblastoma, Cancer Res. 65 (2005) 1678–1686.
[16] D.L. Coppock, A.B. Pardee, Control of thymidine kinase mRNA during the cell cycle, Mol. Cell. Biol. 7 (1987) 2925–2932.
[17] R. Hamanaka, M.R. Smith, P.M. O'Connor, S. Maloid, K. Mihalic, J.L. Spivak, D.L. Longo, D.K. Ferris, Polo-like kinase is a cell cycle-regulated kinase activated during mitosis, J. Biol. Chem. 270 (1995) 21086–21091.
[18] I.S. Kim, D.H. Kim, S.M. Han, M.U. Chin, H.J. Nam, H.P. Cho, S.Y. Choi, B.J. Song, E.R. Kim, Y.S. Bae, Y.H. Moon, Truncated form of importin α identified in breast cancer cell inhibits nuclear import of p53, J. Biol. Chem. 275 (2000) 23139–23145.

[19] F. Rodicker, B.M. Putzer, p73 is effective in p53-null pancreatic cancer cells resistant to wild-type TP53 gene replacement, Cancer Res. 63 (2003) 2737–2741.
[20] K.E. Knudsen, D. Booth, S. Naderi, Z. Sever-Chroneos, A.F. Fribourg, C. Hunton, J.R. Feramisco, J.Y.J. Wang, E.S. Knudsen, RB-dependent S-phase response to DNA damage, Mol. Cell. Biol. 20 (2000) 7751–7763.
[21] M. Hollstein, M. Hergenhahn, Q. Yang, H. Bartsch, Z.Q. Wang, P. Hainaut, New approaches to understanding p53 gene tumor mutation spectra, Mutat. Res. 431 (1999) 199–209.
[22] M. Kaghad, H. Bonnet, A. Yang, L. Creancier, J.C. Biscan, A. Valent, A. Minty, P. Chalon, J.M. Lelias, X. Dumont, P. Ferrara, F. McKeon, D. Caput, Monoallelically expressed gene related to p53 at 1p36, a region frequently deleted in neuroblastoma and other human cancers, Cell 90 (1997) 809–819.
[23] M.E. Lomax, D.M. Barnes, T.R. Hupp, S.M. Picksley, R.S. Camplejohn, Characterization of p53 oligomerization domain mutations isolated from Li-Fraumeni and Li-Fraumeni like family members, Oncogene 17 (1998) 643–649.
[24] J.C. Bourdon, K. Fernandes, F. Murray-Zmijewski, G. Liu, A. Diot, D.P. Xirodimas, M.K. Saville, D.L. Lane, p53 isoforms can regulates p53 transcriptional activity, Genes Dev. 19 (2005) 2122–2137.
[25] D. Goldschneider, E. Horvilleur, L.F. Plassa, M. Guillaud-Bataille, K. Million, E. Wittmer-Dupret, G. Danglot, H. de The, J. Benard, E. May, S. Douc-Rasy, Expression of C-terminal deleted p53 isoforms in neuroblastoma, Nucleic Acids Res. 34 (2006) 5603–5612.
[26] N. Arai, D. Nomura, K. Yokota, D. Wolf, E. Brill, O. Shohat, V. Rotter, Immunologically distinct p53 molecules generated by alternative splicing, Mol. Cell. Biol. 6 (1986) 3232–3239.

Development 134, 579-590 (2007) doi:10.1242/dev.02747

Mammalian Polycomb Scmh1 mediates exclusion of Polycomb complexes from the XY body in the pachytene spermatocytes

Yuki Takada[1], Kyo-ichi Isono[1], Jun Shinga[1], James M. A. Turner[2], Hiroshi Kitamura[1], Osamu Ohara[1], Gen Watanabe[3], Prim B. Singh[4], Takehiko Kamijo[5], Thomas Jenuwein[6], Paul S. Burgoyne[2] and Haruhiko Koseki[1,*]

The product of the Scmh1 gene, a mammalian homolog of *Drosophila* Sex comb on midleg, is a constituent of the mammalian Polycomb repressive complexes 1 (Prc1). We have identified Scmh1 as an indispensable component of the Prc1. During progression through pachytene, Scmh1 was shown to be excluded from the XY body at late pachytene, together with other Prc1 components such as Phc1, Phc2, Rnf110 (Pcgf2), Bmi1 and Cbx2. We have identified the role of Scmh1 in mediating the survival of late pachytene spermatocytes. Apoptotic elimination of *Scmh1*$^{-/-}$ spermatocytes is accompanied by the preceding failure of several specific chromatin modifications at the XY body, whereas synapsis of homologous autosomes is not affected. It is therefore suggested that Scmh1 is involved in regulating the sequential changes in chromatin modifications at the XY chromatin domain of the pachytene spermatocytes. Restoration of defects in *Scmh1*$^{-/-}$ spermatocytes by *Phc2* mutation indicates that Scmh1 exerts its molecular functions via its interaction with Prc1. Therefore, for the first time, we are able to indicate a functional involvement of Prc1 during the meiotic prophase of male germ cells and a regulatory role of Scmh1 for Prc1, which involves sex chromosomes.

KEY WORDS: Mouse, Polycomb, Scmh1, Spermatogenesis, Apoptosis, XY body

INTRODUCTION

The Polycomb group (PcG) genes were first identified by their requirement for the maintenance of the stable repression of Hox genes during the development of *Drosophila melanogaster* (Jürgens, 1985; Paro, 1995; Pirrotta, 1997). *Drosophila* PcG gene products form large multimeric protein complexes and are thought to act by changing the local chromatin structure, as suggested by the synergistic genetic interactions between mutant alleles of different *Drosophila* PcG genes (Jürgens, 1985; Franke et al., 1992; Paro, 1995; Pirrotta, 1997; Shao et al., 1999). In mammals, genes structurally and functionally related to *Drosophila* PcG genes have been identified and mammalian PcG gene products form several distinct complexes. Polycomb repressive complex-2 (Prc2), which contains the product of Eed (the ortholog of the *Drosophila* extra sex combs gene), Ezh2 (the ortholog of the *Drosophila* enhancer of zeste gene) and Suz12, mediates trimethylation of histone H3 at K27 (H3-K27) by Ezh2 component (Schumacher et al., 1996; Laible et al., 1997; van Lohuizen et al., 1998; Sewalt et al., 1998; van der Vlag and Otte, 1999). The second complex, which is closely related to the Polycomb repressive complex-1 (Prc1) in *Drosophila*, includes the products of the paralogs of class 2 PcG genes (Levine et al., 2002). This subset contains gene groups, namely *Pcgf2* (also known as *Rnf110* and *Mel18*, and hereafter referred to as *Rnf110*) and *Bmi1*, *Cbx2* (also known as *M33*), *Cbx4* (also known as *MPc2*) and *Cbx8* (also known as *Pc3*), *Phc1* (also known as *rae28*), *Phc2* and *Phc3*, *Ring1* and *Rnf2* (also known as *Ring1B*) (Levine et al., 2002). The Prc1 complex is compositionally and functionally conserved between flies and mammals (Shao et al., 1999; Levine et al., 2002; Gebuhr et al., 2000). In mammals, chromatin binding of Prc1 involves its recognition of trimethylated H3-K27 (Boyer et al., 2006; Lee et al., 2006; Fujimura et al., 2006). The Prc1 complex has a significant impact on the control of not only anteroposterior (AP) specification of the axis via Hox regulation, but also the proliferation and senescence via regulation of the Ink4a/p53 pathway (Jacobs et al., 1999).

Sex comb on midleg (*Scm*) gene is a member of *Drosophila PcG* genes and, based on database comparison, its product contains three separable functional domains (Bornemann et al., 1996), namely: a pair of N-terminal zinc fingers, two tandem 100-amino acid repeats, called mbt repeats as they are also found in the fly tumor suppressor encoded by the *l(3)mbt* [*lethal(3) malignant brain tumor*] gene, and C-terminal homology domain of 65 amino acids, called the SPM domain. The SPM domain is a self-binding protein interaction module and may mediate Scm association to Prc1 and play a key role for PcG repression, although Scm association to purified Prc1 is substoichiometric (Levine et al., 2002). In mammals, there are four paralogs for *Drosophila Scm* based on primary sequence: *Scmh1*, *Scml1*, *Scml2* and *Sfmbt* (Tomotsune et al., 1999; van de Vosse et al., 1998; Montini et al., 1999; Usui et al., 2000). The mammalian Scmh1 protein has been shown to be a constituent of the mammalian Prc1 (Levine et al., 2002), which contains two highly conserved motifs, two mbt repeats in the N-terminal region and an SPM domain in the C-terminal region, that are shared with its *Drosophila* counterpart. The SPM domain of Scmh1 can mediate its

[1]RIKEN Research Center for Allergy and Immunology, 1-7-22 Suehiro, Tsurumi-ku, Yokohama 230-0045, Japan. [2]Division of Stem Cell Research and Developmental Genetics, MRC National Institute for Medical Research, The Ridgeway, Mill Hill, London NW7 1AA, UK. [3]Laboratory of Veterinary Physiology, Tokyo University of Agriculture and Technology, Fuchu, Tokyo 183-8509, Japan. [4]Nuclear Reprogramming Laboratory, Division of Gene Expression and Development, Roslin Institute (Edinburgh), Roslin, Midlothian EH25 9PS, UK. [5]Department of Pediatrics, Shinshu University School of Medicine, Matsumoto, Nagano 390-8621, Japan. [6]Research Institute of Molecular Pathology, The Vienna Biocenter, Dr Bohrgasse 7, A-1030 Vienna, Austria.

*Author for correspondence (e-mail: koseki@rcai.riken.jp)

Accepted 17 November 2006

interaction with *Drosophila* polyhomeotic (Ph) and mammalian Phc1 and Phc2, through their respective SPM domains (Tomotsune et al., 1999). It is also notable that tissue-specific *Scmh1* mRNA levels in the testes are the highest of all tissues analyzed and they increase during the synchronous progression of first-wave spermatogenesis in parallel with *Phc1* (see Fig. S1A,B in the supplementary material). These observations suggest a role of mammalian Prc1 during spermatogenesis.

Before the specialized cell division of meiosis, postmitotic spermatocytes enter into an extended meiotic prophase, in which homologous autosomal chromosomes pair and undergo reciprocal recombination. There is accumulating evidence to suggest that the quality of this complex process is monitored by a checkpoint to ensure spermatogenic success, as represented by the apoptotic elimination of those spermatocytes with synaptic errors. During this period, heteromorphic sex chromosomes pair only in a small pseudoautosomal region (PAR) at their distal ends and undergo transcriptional inactivation, termed meiotic sex chromosome inactivation (MSCI), by remodeling into heterochromatin, thus forming the XY body (Perry et al., 2001; Odorisio et al., 1996; Singer-Sam et al., 1990; Turner et al., 2004; Baarends et al., 1999; Strahl and Allis, 2000; Turner et al., 2000; Hoyer-Fender et al., 2000; Mahadevaiah et al., 2001; Khalil et al., 2004). Formation of the XY body is conserved throughout the mammalian phylogenetic tree and is therefore assumed to be essential for successful spermatogenesis and the faithful segregation of sex chromosomes. Indeed, in mutants for the gene encoding histone H2A.X and the tumor suppressor protein Brca1, failure to form the XY body coincides with sterility due to the apoptotic elimination of such mutant spermatocytes before completion of meiosis (Fernandez-Capetillo et al., 2003; Xu et al., 2003). However, it has not been definitely demonstrated that spermatogenic arrest in these mutants is because of failure to form the XY body or due to some other reason. The condensation of the X and Y chromosome to form the XY body is associated with post-translational modifications of histones and the recruitment or exclusion of various chromatin-associated proteins (Turner et al., 2001; Hoyer-Fender et al., 2000; Richler et al., 2000; Mahadevaiah et al., 2001; Khalil et al., 2004; Baarends et al., 1999; Baarends et al., 2005). Early in the formation of the XY body, phosphorylated histone H2A.X (γH2A.X) and ubiquitylated histone H2A (uH2A) are enriched at the XY body and then X and Y chromosomes undergo sequential changes in their histone modifications, which correlate with transcriptional status of sex chromosomes (Mahadevaiah et al., 2001; Baarends et al., 1999; Baarends et al., 2005). The functional involvement of these histone modifications at the XY body was properly addressed for the first time in a study using *Brca1* mutants, in which H2A.X phosphorylation was shown to be essential to trigger MSCI (Turner et al., 2004). However, the roles of hyperubiquitylation of H2A on the X and Y chromosomes have still not been addressed. Recent studies have revealed an Rnf2 component of Prc1 to be an E3 component of ubiquitin ligase for histone H2A to link Prc1 with the XY body (de Napoles et al., 2004; Baarends et al., 1999; Baarends et al., 2005).

In this study, we have generated a mouse line carrying a mutant *Scmh1* allele that lacks the exons to encode an SPM domain. Axial homeotic transformations and premature senescence in mouse embryonic fibroblasts (MEFs) in the homozygotes indicated the role of Scmh1 as a PcG component. Approximately half the $Scmh1^{-/-}$ males were infertile, which correlates with an accelerated apoptosis of postmitotic pachytene spermatocytes. The present genetic study indicates the involvement of Prc1 during XY body maturation and the regulatory role of Scmh1 gene products in the exclusion of Prc1 from the XY body, which may in turn be required for the further progression of meiotic prophase.

MATERIALS AND METHODS

Mice

Scmh1-deficient mice were generated using R1 embryonic stem (ES) cells according to the conventional protocol and backcrossed to C57BL/6 background four to six times (Akasaka et al., 1996). Schematic representations of genomic organization and targeting vector are shown in Fig. S2 in the supplementary material. *Scmh1* mutant mice were genotyped by PCR using the following oligonucleotides: (a) 5′-GTCAG-GTGTGCCCGCTACTGT-3′ and (b) 5′-GATGGATTGCACGCAGGTTC-3′ for the mutant allele; and (a) and (c) 5′-GGCCGACTAGGC-CATCTTCTG-3′ for the *Scmh1* wild-type allele. As *Scmh1* and *Phc2* loci were on chromosome 4 and 28×10^6 base pairs (bp) apart from each other, we first generated recombinants in which *Scmh1* and *Phc2* mutant alleles were physically linked. This double mutant allele was used to generate *Scmh1;Phc2* double homozygotes. Skeletal analysis was performed as described previously (Kessel and Gruss, 1991). MEFs were maintained according to a 3T9 protocol as described previously (Kamijo et al., 1997).

In situ hybridization, RT-PCR and immunohistochemistry

In situ hybridization was performed as described previously (Yuasa et al., 1996). The nucleotide sequences of the primers used for RT-PCR in this study are listed in Table 1. Immunohistochemistry was performed as described previously (Hoyer-Fender et al., 2000).

TUNEL staining

Apoptotic cells were visualized by the terminal deoxynucleotidetransferase-mediated dUTP nick end-labeling (TUNEL) assay (In Situ Cell Death Detection Kit, AP; Roche, Germany).

Immunocytochemistry of spread spermatocytes

Meiotic prophase cell spreads and squashes were prepared as described previously (Scherthan et al., 2000). After washing with PBS for 3 minutes, slides bearing cell spreads were processed for immunostaining using standard procedures. The antibodies used for immunostaining in this study are listed in Table 2. For the statistical analyses, 300 spermatocytes derived from five mice with respective genotypes were analyzed and the significance was further analyzed by *t*-test.

Microarray analysis

Microarray analysis was performed using Mouse Genome 430 2.0 GeneChips (Affymetrix, Santa Clara, CA) according to the manufacturer's instructions. The intensity for each probe set was calculated using the MAS5 method of the GCOS software package (Affymetrix) at the default setting. Per chip normalization was performed using a median correction program in the GeneSpring software package (Agilent Technologies, Palo Alto, CA). One comparison between the two groups was conducted using a triplicate array. Data of probe sets were excluded from the analyses when they were judged to be 'absent' by the GCOS program in at least one sample in the stimulated groups. Probe sets that differentially hybridized between the samples were identified by the following criteria: (1) Welch's analysis of variance (ANOVA) showed that the *P*-value was less than 0.05; (2) the Benjamini and Hochberg false discovery test confirmed the ANOVA result; and (3) more than a twofold difference in the expression levels was observed between the samples.

RESULTS

Scmh1 is a functional component of PcG complexes

We generated a mutant allele for Scmh1 by deleting the sequences encoding the SPM domain, in which a small amount of truncated *Scmh1* transcript was expressed (see Fig. S2A-E in the supplementary material). As the *Drosophila* Scm^{XF24} allele, in which the SPM domain is exclusively affected, presents an almost identical phenotype to null alleles, the *Scmh1* mutant allele could be a null or

Table 1. Primers used in semiquantitative RT-PCR analyses

Gene	Forward (5'→3')	Reverse (5'→3')
A-myb	aagaagttggttgaacaacacgg	aggaagtaacttagcaatctcgg
Dmc1	ttcgtactggaaaaactcagctgtatc	cttggctgcgacataatcaagtagctcc
Mvh1	ccaaaagtgacatatataccc	ttggttgatcacttctcgag
Scp-3	ggtggaagaaagcattctgg	cagctccaaatttttccagc
CyclinA1	atgcatcgccagagctccaagag	ggaagtggagatctgacttgagc
Calmegin	atatgcgtttccagggtgttggac	gtatgcacctccacaatcaatacc
Bmp8a	ggctcgagatggtggtcaaggcctgtgg	ggggatccaggctctttctatgtggcc
CREMτ	gattgaagaagaaaaatcaga	catgctgtaatcagttcatag
β-actin	gagagggaaatcgtgcgtga	acatctgctggaaggtggac
Scmh1		
Primers 1/2	atgctggtttgctac	aggacaaaggtttcacct
Primers 3/4	actgccacagagtataatca	tcagaacttgccctg

Table 2. Antibodies used in immunostaining analyses

Antibody	Species	Dilution	Company
Anti-p53(clone pAb421)	Rabbit	1:500	Oncogene Research Products
Anti-Scp3	Rabbit	1:100	Novus Biologicals
Anti-phospho-H2A.X (Ser139)	Rabbit	1:500	Upstate
Anti-ubiquityl-Histone H2A(clone E6C5)	Mouse	1:100	Upstate
Anti-monomethyl-Histone H3(Lys9)	Rabbit	1:100	Upstate
Anti-dimethyl-Histone H3(Lys9)	Rabbit	1:100	Upstate
Anti-acetyl-Histone H3	Rabbit	1:100	Upstate
Anti-trimethyl-Histone H3 (Lys27)	Rabbit	1:100	Upstate
Anti-dimethyl-Histone H4 (Lys20)	Rabbit	1:100	Upstate
Anti-monomethyl-Histone H3 (Lys4)	Rabbit	1:100	Upstate
Anti-Rad51 (H-92)	Rabbit	1:50	Santa Cruz
Anti-Mlh1 (G168-15)	Mouse	1:50	BD Pharmingen
Anti-phosphorylated RNA polymerase II	Mouse	1:25	Covance
Anti-Scmh1	Mouse	Undiluted	This study
Anti-Phc1	Mouse	Undiluted	Miyagishima et al., 2003
Anti-Phc2	Mouse	Undiluted	Isono et al., 2005
Anti-Bmi1(H-99)	Rabbit	1:25	Santa Cruz
Anti-Rnf110(C-20)	Rabbit	1:30	Santa Cruz
Anti-Cbx2(C-18)	Rabbit	1:25	Santa Cruz
Anti-Rnf2	Mouse	Undiluted	Atsuta et al., 2001
Anti-Ezh2	Rabbit	1:100	Upstate
Anti-mouse IgM FITC	Donkey	1:100	Becton Dickinson
Anti-mouse IgG Cy2	Donkey	1:100	Jackson ImmunoResearch Laboratories
Anti-rabbit IgG Cy3	Donkey	1:500	Jackson ImmunoResearch Laboratories
Anti-mouse IgG (H+L) Alexa Fluor 488	Goat	1:300	Molecular Probes
Anti-rabbit IgG (H+L) Alexa Fluor 568	Goat	1:300	Molecular Probes
Anti-rabbit IgG, HRP-conjugated	Goat	1:2000	Amersham

strong hypomorphic mutation (Bornemann et al., 1996). Although both male and female *Scmh1*$^{-/-}$ mice were viable and grew normally to adulthood, homozygotes exhibited the axial homeosis and premature senescence of MEFs in the homozygous mutants, which was restored by the *p19*^{ARF} or *p53* mutation (see Fig. S2F-K in the supplementary material). Therefore, Scmh1 is an indispensable component of Prc1 in mice.

The expression and subcellular localization of Scmh1 during spermatogenesis

About half the homozygotes were sterile and had slightly smaller testes than their wild-type littermates (Y.T., unpublished). Before studying the pathogenesis of infertility in *Scmh1* mutants, we examined Scmh1 expression during spermatogenesis by in situ hybridization and immunohistochemical analysis. *Scmh1* expression was seen in the seminiferous tubules and interstitial cells (Fig. 1Aa). In the seminiferous tubules, morphological examination of the germ cell layers representing meiotic spermatocytes (particularly those at the pachytene stage) revealed that these germ layers were expressing the highest amount of *Scmh1*, with the least amounts expressed in spermatogonia and round spermatids (Fig. 1Ab). Sertoli cells also expressed a significant amount of *Scmh1*. By using an immunohistochemical technique, a light staining of the whole nucleus was observed in the zygotene stage and in more advanced cells up to pachytene spermatocytes (Fig. 1Ba). In addition, focal localization of Scmh1 was seen in the chromocenter of round spermatids (Fig. 1Bb). Concordantly, *Scmh1* expression in the testes correlated with synchronous progression of the first-wave spermatogenesis (see Fig. S1B in the supplementary material). From day 15 post partum (pp) onwards, the amount of *Scmh1* transcript progressively increased and reached a maximum level by day 25 pp. Taken together, *Scmh1* and its products are predominantly expressed in postmitotic spermatocytes.

We went on to investigate subcellular localization of Scmh1 by using spread meiotic spermatocytes. The synaptonemal complex protein Scp3, which is a component of the axial element, was used to substage meiosis (Xu et al., 2003). Scmh1 staining was seen in the nucleus as a diffused pattern from leptotene to early pachytene spermatocytes (Fig. 1Ca-c and Y.T., unpublished). In late pachytene spermatocytes, Scmh1 staining was significantly excluded from the

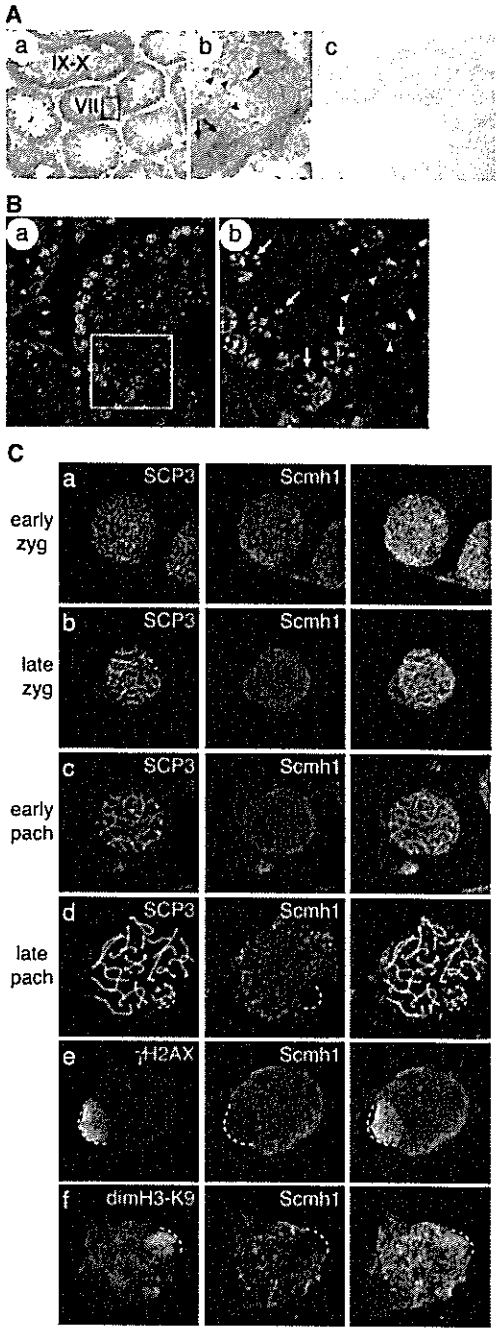

Fig. 1. Localization of Scmh1 in the adult testes and spermatocytes. (**Aa**) In situ hybridization using antisense probe. Stages of seminiferous tubules are given. (**Ab**) Higher magnification view of seminiferous tubule at stage VII shown in a. Arrows and arrowheads indicate pachytene spermatocytes and round spermatids, respectively. (**Ac**) Control slides using sense probe. (**Ba**) Immunohistochemical localization of Scmh1 of wild-type testes. (**Bb**) Higher magnification view of seminiferous tubule shown in a. Arrows and arrowheads indicate pachytene spermatocytes and round spermatids, respectively. (**C**) Immunocytochemical detection of Scmh1 gene products from zygotene to pachytene stage spermatocytes, which were prepared from day 18 pp wild-type testes. (**Ca-Cd**) Spermatocyte spreads were substaged into early (a) and late (b) zygotene and early (c) and late (d) pachytene stages based on anti-Scp3 (red) immunostaining and morphology. Scmh1 (green) was localized in the nuclei at each stage, but was mostly excluded from the X and Y chromosome territory at late pachytene stage, as indicated by dotted lines. (**Ce**) Reciprocal subnuclear localization of Scmh1 and γH2A.X indicated exclusion of Scmh1 from the XY body. The XY body is indicated by dotted lines. (**Cf**) Reciprocal subnuclear localization of Scmh1 and dimethylated H3-K9 indicated exclusion of Scmh1 from the XY body. The XY body is indicated by dotted lines.

XY chromatin domain (Fig. 1Cd,e). Concordantly, reciprocal localization of Scmh1 and γH2A.X was seen in about 80% of pachytene spermatocytes (Fig. 1Ce). Consistently, Scmh1 was excluded from the XY body in which dimethylated histone H3 at K9 (H3-K9) was enriched (Fig. 1Cf).

Subcellular localization of PcG proteins and trimethylated H3-K27 during spermatogenesis

The progressive exclusion of Scmh1 from the XY body during the pachytene stage prompted us to examine the subcellular localization of other PcG proteins and trimethylated H3-K27, which is mediated by the Ezh2 component of Prc2. Subcellular localization of Phc1, Phc2, Bmi1, Rnf110 and Cbx2 were compared with γH2A.X or uH2A. Reciprocal localization of these PcG proteins and γH2A.X or uH2A, within about 80% of spermatocytes, indicated the exclusion of other PcG proteins from the XY body during the pachytene stage, as well as Scmh1 (Fig. 2Aa-e). Consistently, Phc2 was excluded from the XY body in 77% of spermatocytes, in which dimethylated H3-K9 was enriched (Fig. 2Af). Taken together, PcG complexes are excluded from the XY body at the late pachytene stage almost concurrently with hyperdimethylation of H3-K9 at the XY body, whereas they are continuously present in the autosomal regions.

Recent studies have repeatedly provided evidence indicating the engagement of Prc1 by trimethylated H3-K27 mediated by Prc2 (Cao et al., 2002; Kuzmichev et al., 2002). We thus addressed whether the exclusion of Prc1 components from the XY body was correlated with the degree of H3-K27 trimethylation at the XY chromatin domain. Trimethylated H3-K27 was distributed throughout the nucleus as a diffuse pattern from leptotene to zygotene stage spermatocytes despite the fact that the signals were very dim (Fig. 2Ba and Y.T., unpublished). In early pachytene spermatocytes, trimethylated H3-K27 staining was much stronger than in the earlier stages but was significantly excluded from the XY chromatin domain (Fig. 2Bb). In late pachytene spermatocytes, its exclusion from the XY body was still maintained (Fig. 2Bc). Therefore the exclusion of trimethylated H3-K27 from the XY chromatin domain precedes those of Prc1 components.

Impaired spermatogenesis in *Scmh1*$^{-/-}$ males

We first examined the histology of *Scmh1*$^{-/-}$ testes in day 35 pp testes and revealed that about two-thirds were morphologically altered to varying extents. The seminiferous tubules of *Scmh1*$^{-/-}$ testes exhibited a reduction in the number of spermatocytes and a lack of spermatids and mature spermatozoa (Fig. 3Aa,b). Sertoli cells and spermatogonia were morphologically and numerically normal. Mono- or multinuclear large cells were sometimes seen. One-third of *Scmh1*$^{-/-}$ testes were morphologically indistinguishable from wild type. Therefore, spermatogenesis was variably affected in *Scmh1*$^{-/-}$ testes.